7 Phonon Drag in High Landau Levels

Our study of phonon drag in high Landau levels builds on previous work on Coulomb drag in this regime [86]. The principal differences are: (i) the linear response theory for drag has to be extended to large momentum transfers $q \sim 2k_F$, (ii) instead of direct Coulomb interaction, the phonon-mediated interlayer interaction has to be included. The linear response theory for frictional drag has already been introduced in Section 6.4. In Section 7.1, we present the extension of this linear response theory to arbitrary momentum transfers q. The electron-phonon interaction in bilayer systems is derived in Section 7.2. Analytical and numerical results for phonon drag are provided in Sections 7.3 and 7.4, respectively.

7.1 Linear Response Theory of Phonon Drag: Triangle Vertex and Polarization Function

7.1.1 Relevant Momentum Range and Regime of Interest

For Coulomb drag, the interlayer interaction is suppressed at large momentum transfers q by a factor e^{-qd}. Hence, the Coulomb drag contribution to the transconductivity is governed by small momentum transfers $q < 1/d$. Over length scales small compared to the cyclotron radius R_c, electron transport is ballistic, while over length scales large compared to R_c, it is diffusive. Thus, if the interlayer separation d satisfies $d \gg R_c$ (diffusive regime), only "diffusive" momenta $qR_c \ll 1$ contribute to the drag conductivity. On the other hand, for $d \ll R_c$ (ballistic regime), both "ballistic" momenta $qR_c \gg 1$ and "diffusive" momenta contribute [86]. The latter case is relevant for Coulomb drag in high Landau levels since the condition $R_c > d$ is typically satisfied in drag measurements.

By contrast, in phonon drag there is no suppression of large momentum transfers by the interaction. The only momentum cutoff stems from temperature. At temperatures in the vicinity of T_{bs}, momenta up to $q \sim 2k_F$ contribute to the drag conductivity. In this situation the contribution of small (diffusive) momenta is negligible with respect to the contribution of large (ballistic) momenta.[1] We therefore omit a discussion of diffusive momenta and restrict ourselves to the analysis of ballistic momenta

$$\frac{1}{qR_C} \ll 1 \quad . \tag{7.1}$$

[1] This effect is further enhanced by the specific form of the phonon-mediated electron-electron interaction, which is peaked at large momentum transfers $q \sim 2k_F$.

A realistic estimate for the backscattering temperature is $T_{bs} = 2ck_F \simeq 1\mathrm{K}$, where c is the phonon sound velocity. Since $\omega_c \simeq 10\mathrm{K} \times B[\mathrm{T}]$ and, in drag experiments, magnetic fields are of the order $B \simeq 1\mathrm{T}$, it is reasonable to assume

$$T_{bs} \ll \Delta \ll \omega_c \quad , \tag{7.2}$$

where Δ is the Landau level broadening. We focus on the regime of well-separated Landau levels ($\Delta/\omega_c \ll 1$). We also assume that the Fermi energy is in a high LL of index $N \gg 1$. While limiting ourselves to temperatures T of the order of T_{bs} or below in all analytical derivations, we will overcome this limitation for the numerical treatment presented in Section 7.4.

7.1.2 Triangle Vertex: Dominant Contribution $\mathbf{\Gamma}^{(q/k_F)}$

We now proceed to the calculation of the dominant contribution to the triangle vertex $\mathbf{\Gamma}$ in the regime of interest specified above. $\mathbf{\Gamma}$ will be treated in SCBA, since this is a controlled approximation for high Landau levels $N \gg 1$. Within SCBA, there are no vertex corrections to the vector vertex. Since the bare current vertex couples neighboring LLs only, when performing the trace in Eqs. (6.9-6.10) two of the three Green functions in the triangle vertex have to be evaluated in the valence LL of index N, while the third has to be evaluated in the $(N \pm 1)$st LL.

For the treatment of phonon drag, we need the triangle vertex $\mathbf{\Gamma}$ for large momenta. Consequently, it is appropriate to neglect contributions to $\mathbf{\Gamma}$ from the diffusive regime of momenta. In this ballistic limit, it turns out that to leading order in $1/qR_c$ the longitudinal components (parallel to $\mathbf{q}$) of $\mathbf{\Gamma}^{(a)}$ and $\mathbf{\Gamma}^{(b)}$ cancel each other. The main contribution to the triangle vertex thus stems from the transverse component of $\mathbf{\Gamma}^{(b)}$.

The starting point for our calculation is Eq. (6.10). Fixing the x-axis to point along the direction of $\mathbf{q}$,

$$\mathbf{q} = q\mathbf{e}_x \quad , \tag{7.3}$$

the transverse part of $\mathbf{\Gamma}^{(b)}$ (parallel to $\mathbf{e}_y = \mathbf{e}_z \times \hat{\mathbf{q}}$) is given by

$$\mathbf{\Gamma}_t^{(b)}(\mathbf{q},\omega) = \frac{\omega}{i\pi}\mathbf{e}_y \mathrm{tr}\Big\{ v_y \mathcal{G}^-(E_F) e^{i\mathbf{qr}} [\mathcal{G}^-(E_F) - \mathcal{G}^+(E_F)] e^{-i\mathbf{qr}} \mathcal{G}^+(E_F) \Big\} \quad . \tag{7.4}$$

When performing the trace, the specific form of the v_y matrix element necessitates that one of the three Green functions of the product in the above expression be evaluated in a different Landau level than the other two. Since the Green function matrix element[2] $G_N^{\pm}$ is larger by a factor ω_c than the matrix elements $G_{N\pm1}^{\pm}$, the leading contribution to $\mathbf{\Gamma}_t^{(b)}$, which will be denoted by

[2] For the explicit expression for $G_N^{\pm}$, see Appendix D.

$\mathbf{\Gamma}^{(q/k_F)}$, is given by[3]

$$\begin{aligned}\mathbf{\Gamma}^{(q/k_F)}(\mathbf{q},\omega) &= \frac{\omega}{i\pi}\mathbf{e}_y \sum_{n=N\pm1} \\ &\Big\{\langle N|v_y|n\rangle G_n^- \langle n|e^{i\mathbf{qr}}|N\rangle [G_N^- - G_N^+]\langle N|e^{-i\mathbf{qr}}|N\rangle G_N^+ \\ &+\langle n|v_y|N\rangle G_N^- \langle n|e^{i\mathbf{qr}}|N\rangle [G_N^- - G_N^+]\langle N|e^{-i\mathbf{qr}}|n\rangle G_n^+\Big\}. \quad (7.5)\end{aligned}$$

The matrix elements appearing in Eq. (7.5) can be evaluated using the expressions provided in Appendix D. For better readability, we introduce a vertex overlap function

$$\mathcal{L}_\sigma^j(q\ell_B) = \left(\frac{q\ell_B}{\sqrt{2N}}\right)^j e^{-q^2\ell_B^2/2} L_{N-\sigma}^j\left(\frac{(q\ell_B)^2}{2}\right) L_N^0\left(\frac{(q\ell_B)^2}{2}\right) \quad , \qquad (7.6)$$

where $j,\sigma \in \{0,1\}$. For $j=1$, this function simply corresponds to the vertex overlap $\langle N|e^{i\mathbf{q}\cdot\mathbf{r}}|N\rangle\langle N|e^{-i\mathbf{q}\cdot\mathbf{r}}|N-\sigma\rangle$. For later convenience, we also introduced the case $j=0$. In terms of this vertex overlap function, $\mathbf{\Gamma}^{(q/k_F)}$ takes the form

$$\begin{aligned}\mathbf{\Gamma}^{(q/k_F)}(\mathbf{q},\omega) &= \frac{\omega\sqrt{2N}}{2\pi m\ell_B}\mathbf{e}_y \left(G_N^- - G_N^+\right)\left\{\mathcal{L}_0^1(q\ell_B)\left[G_N^- G_{N+1}^+ - G_N^+ G_{N+1}^-\right]\right. \\ &\left. -\mathcal{L}_1^1(q\ell_B)\left[G_N^- G_{N-1}^+ - G_N^+ G_{N-1}^-\right]\right\} \quad . \qquad (7.7)\end{aligned}$$

Expanding the matrix elements $G_{N\pm1}^\pm$ to first order in Δ/ω_c and using

$$(G_N^+ - G_N^-)^2 = -16\frac{\Delta^2 - (E_N - E_F)^2}{\Delta^4} \quad , \qquad (7.8)$$

this yields for the main contribution to the triangle vertex

$$\begin{aligned}\mathbf{\Gamma}^{(q/k_F)}(\mathbf{q},\omega) &= (\mathbf{e}_z\times\hat{\mathbf{q}})\frac{\omega\, R_c}{\pi^2\ell_B^2}(G_N^+ - G_N^-)^2 \sum_{\sigma\in\{0,1\}}(-1)^\sigma\, \mathcal{L}_\sigma^1(q\ell_B) \\ &= -16(\mathbf{e}_z\times\hat{\mathbf{q}})\frac{\omega\, R_c}{\pi^2\ell_B^2}\frac{\Delta^2 - (E_N - E_F)^2}{\Delta^4} \\ &\quad\times \sum_{\sigma\in\{0,1\}}(-1)^\sigma \mathcal{L}_\sigma^1(q\ell_B) \quad . \qquad (7.9)\end{aligned}$$

Using the relation for the difference of generalized Laguerre polynomials [76]

$$L_N^1(x) - L_{N-1}^1(x) = L_N^0(x) \quad , \qquad (7.10)$$

[3] We do not detail the k-integration involved in the trace since it turns out that it is trivial. We also suppress k in the state ket $|Nk\rangle \equiv |N\rangle$ and the argument E_F of the Green function matrix elements.

the sum appearing in Eq. (7.9) can be written as

$$\begin{aligned}\sum_{\sigma\in\{0,1\}}(-1)^\sigma\mathcal{L}^1_\sigma(q\ell_B) &= \mathcal{L}^1_0(q\ell_B)-\mathcal{L}^1_1(q\ell_B)\\ &= \frac{q\ell_B}{\sqrt{2N}}e^{-\frac{q^2\ell_B^2}{2}}L_N^0\left(\frac{q^2\ell_B^2}{2}\right)\\ &\quad\times\quad\left[L_N^1\left(\frac{q^2\ell_B^2}{2}\right)-L_{N-1}^1\left(\frac{q^2\ell_B^2}{2}\right)\right]\\ &= \frac{q\ell_B}{\sqrt{2N}}\mathcal{L}^0_0(q\ell_B)\quad,\end{aligned}\tag{7.11}$$

so that the dominant contribution to the triangle vertex is finally given by[4]

$$\mathbf{\Gamma}^{(q/k_F)}(\mathbf{q},\omega)=-\frac{16\omega}{\pi^2}\frac{\Delta^2-(E_N-E_F)^2}{\Delta^4}\mathcal{L}^0_0(q\ell_B)(\mathbf{e}_z\times\mathbf{q})\quad.\tag{7.12}$$

Additional contributions will be discussed in Section 7.1.4.

7.1.3 The Polarization Function in the Ballistic Regime

This section is devoted to the calculation of the polarization function $\chi(q,\omega)$, which will be needed for a proper treatment of screening effects in Section 7.3. In addition, $\chi(q,\omega)$ is closely related to the triangle vertex, as will be shown below.

Accounting for the spin degree of freedom and neglecting vertex corrections, the polarization bubble can be written in Matsubara representation as [92]

$$\begin{aligned}\chi(q,i\omega_n) &= -\frac{2T}{S}\sum_{i\epsilon_n}\sum_{m,k}\sum_{m',k'}G_m(i\epsilon_n)G_{m'}(i\epsilon_n+i\omega_n)\\ &\quad\times\langle mk|e^{i\mathbf{q}\cdot\mathbf{r}}|m'k'\rangle\langle m'k'|e^{-i\mathbf{q}\cdot\mathbf{r}}|mk\rangle\quad,\end{aligned}\tag{7.13}$$

where G_m is the (impurity-averaged) Green function matrix element in the mth Landau level, S is the area of the sample and $\epsilon_n=2\pi(n+1/2)T$ are fermionic Matsubara frequencies. The Green function matrix elements do not depend on k,k', so that Eq. (7.13) can be simplified to

$$\chi(q,i\omega_n)=-\frac{2T}{\pi\ell_B^2}\sum_{i\epsilon_n}\sum_{m,m'}G_m(i\epsilon_n)G_{m'}(i\epsilon_n+i\omega_n)|f_{mm'}(q)|^2\tag{7.14}$$

with[5]

$$\begin{aligned}|f_{mm'}(q)|^2 = &\quad e^{-\frac{q^2\ell_B^2}{2}}\frac{\min\{m,m'\}!}{\max\{m,m'\}!}\left(\frac{q^2\ell_B^2}{2}\right)^{|m-m'|}\\ &\times\quad\left[L^{|m-m'|}_{\min\{m,m'\}}\left(\frac{q^2\ell_B^2}{2}\right)\right]^2\quad.\end{aligned}\tag{7.15}$$

[4] Note that the term $(\mathbf{e}_z\times\mathbf{q})$ now contains $\mathbf{q}$ instead of $\hat{\mathbf{q}}$.
[5] Note that $|f_{mm'}(q)|^2$ is closely related to $\mathcal{L}^j_\sigma(q\ell_B)$ from Eq. (7.6).

The polarization function can then be obtained via analytic continuation ($i\omega_n \to \omega + i0^+$). Writing the sum over the Matsubara frequencies ϵ_n in Eq. (7.14) as a contour integral and deforming the contour in the standard manner, one obtains

$$\begin{aligned}\chi(q,\omega) &= -\frac{2}{\pi\ell_B^2}\sum_{nm} e^{-\frac{q^2\ell_B^2}{2}} \left[L^{|m-n|}_{\min\{n,m\}}\left(\frac{q^2\ell_B^2}{2}\right)\right]^2 \left(\frac{q^2\ell_B^2}{2}\right)^{|n-m|} \frac{\min\{n,m\}!}{\max\{n,m\}!} \\ &\times \int_{-\infty}^{+\infty} \frac{d\epsilon}{\pi}\, n_F(\epsilon)\, \frac{1}{2}\left\{\left[G_n^-(\epsilon) - G_n^+(\epsilon)\right] G_m^-(\epsilon+\omega)\right. \\ &\qquad \left. + G_n^+(\epsilon-\omega)\left[G_m^-(\epsilon) - G_m^+(\epsilon)\right]\right\} \quad , \end{aligned} \tag{7.16}$$

where $n_F(\epsilon)$ is the Fermi distribution function. This expression can be cast into the form

$$\begin{aligned}\chi(q,\omega) &= -\frac{2}{\pi\ell_B^2}\sum_{nm} e^{-\frac{q^2\ell_B^2}{2}} \left[L^{|m-n|}_{\min\{n,m\}}\left(\frac{q^2\ell_B^2}{2}\right)\right]^2 \left(\frac{q^2\ell_B^2}{2}\right)^{|n-m|} \frac{\min\{n,m\}!}{\max\{n,m\}!} \\ &\times \int_{-\infty}^{+\infty} \frac{d\epsilon}{\pi}\, n_F(\epsilon)\, \mathrm{Im}\left[G_n^-(\epsilon)\right]\, \left[G_m^-(\epsilon+\omega) + G_m^+(\epsilon-\omega)\right] \quad . \end{aligned} \tag{7.17}$$

We will now discuss the real and imaginary parts of $\chi(q,\omega)$ separately.

Real Part of the Polarization Function

The real part of the polarization function

$$\begin{aligned}\mathrm{Re}[\chi(q,\omega)] &= -\frac{2}{\pi\ell_B^2}\sum_{nm} e^{-\frac{q^2\ell_B^2}{2}} \left[L^{|m-n|}_{\min\{n,m\}}\left(\frac{q^2\ell_B^2}{2}\right)\right]^2 \\ &\times \left(\frac{q^2\ell_B^2}{2}\right)^{|n-m|} \frac{\min\{n,m\}!}{\max\{n,m\}!} \\ &\times \int_{-\infty}^{+\infty} \frac{d\epsilon}{\pi}\, n_F(\epsilon)\mathrm{Im}[G_n^-(\epsilon)]\mathrm{Re}[G_m^-(\epsilon+\omega) + G_m^+(\epsilon-\omega)] \end{aligned} \tag{7.18}$$

can be shown to have two qualitatively different contributions, one from the terms $n \neq m$ and the other from the terms $n = m$ in the sums over n and m. These will be called nondiagonal (nd) and diagonal (d), respectively. To leading order in $1/N$, we find for the nondiagonal contribution

$$\Big(\mathrm{Re}[\chi(q,\omega)]\Big)_{\mathrm{nd}} = -\frac{m}{\pi} = -2\nu_0 \quad , \tag{7.19}$$

which simply is the result for the polarization function at zero magnetic field.[6]

In the low-temperature limit $T, \omega \ll \Delta \ll \omega_c$, the diagonal contribution to the real part of the polarization function is given by

$$\Big(\mathrm{Re}[\chi(q,\omega)]\Big)_{\mathrm{d}} = -\frac{8\nu(E_F)}{3}\mathcal{L}_0^0(q\ell_B)\left[1 - \frac{(E_N - E_F)^2}{\Delta^2}\right] \quad , \tag{7.20}$$

where $\nu(\epsilon)$ is the density of states within SCBA (see Appendix D). The real part of the polarization function is then given by the sum of the two contributions from Eqs. (7.19-7.20).

[6] Here, ν_0 is the zero-field density of states per spin (see Appendix D).

Imaginary Part of the Polarization Function

Next, we discuss the imaginary part of the polarization function

$$\begin{aligned}\mathrm{Im}[\chi(q,\omega)] &= -\frac{2}{\pi\ell_B^2}\sum_{nm} e^{-q^2\ell_B^2/2}\left[L^{|m-n|}_{\min\{n,m\}}(\frac{q^2\ell_B^2}{2})\right]^2 \\ &\times\left(\frac{q^2\ell_B^2}{2}\right)^{|n-m|}\frac{\min\{n,m\}!}{\max\{n,m\}!} \\ &\times\int_{-\infty}^{+\infty}\frac{d\epsilon}{\pi}\,[n_F(\epsilon)-n_F(\epsilon+\omega)]\,\mathrm{Im}[G_n^+(\epsilon)]\,\mathrm{Im}[G_m^+(\epsilon+\omega)] \quad . \end{aligned} \tag{7.21}$$

For $\omega \ll \omega_c$, we obtain to lowest order in Δ/ω_c

$$\begin{aligned}\mathrm{Im}[\chi(q,\omega)] &\simeq \frac{8}{\pi\ell_B^2}\frac{1}{\Delta^2}\,\mathcal{L}_0^0(q\ell_B)\int_{E_N-\Delta}^{E_N+\Delta}\frac{d\epsilon}{\pi}\left[n_F\left(\epsilon+\frac{\omega}{2}\right)-n_F\left(\epsilon-\frac{\omega}{2}\right)\right] \\ &\times\,\mathrm{Re}\left[1-\frac{(\epsilon+\omega/2-E_N)^2}{\Delta^2}\right]^{1/2} \\ &\times\,\mathrm{Re}\left[1-\frac{(\epsilon-\omega/2-E_N)^2}{\Delta^2}\right]^{1/2} \quad . \end{aligned}$$

In the low-temperature limit ($T,\omega \ll \Delta \ll \omega_c$), the imaginary part of the polarization function takes the form

$$\mathrm{Im}[\chi(q,\omega)] = -\frac{8}{\pi^2\ell_B^2}\frac{\omega}{\Delta^2}\,\mathcal{L}_0^0(q\ell_B)\left[1-\frac{(E_N-E_F)^2}{\Delta^2}\right] \quad . \tag{7.22}$$

Connection between Triangle Vertex and Polarization Function

In Section 7.1.2, we calculated the dominant contribution $\mathbf{\Gamma}^{(q/k_F)}(\mathbf{q},\omega)$ to the triangle vertex. By comparing it to the imaginary part of the polarization function $\chi(q,\omega)$, it turns out that $\mathbf{\Gamma}^{(q/k_F)}(\mathbf{q},\omega)$ can be expressed as

$$\mathbf{\Gamma}^{(q/k_F)}(\mathbf{q},\omega) = -(\mathbf{e}_z\times\mathbf{q})\frac{2\sigma_{xy}}{e^2 n_e}\mathrm{Im}\chi(q,\omega) \quad , \tag{7.23}$$

where n_e is the electron density and

$$\sigma_{xy} = \frac{en_e}{B} \tag{7.24}$$

is the classical Hall conductivity. This relation is not a mere coincidence, but of very general character [93, 94, 95]. It can be shown [86] that the relation

$$\mathbf{\Gamma}(\mathbf{q},\omega) = -(\mathbf{e}_z\times\mathbf{q})\frac{2\sigma_{xy}}{e^2 n_e}\mathrm{Im}\chi(q,\omega) \tag{7.25}$$

also holds for higher-order (in Δ/ω_c) expansions of the triangle vertex when replacing the classical Hall conductivity with the SCBA result

$$\sigma_{xy} = \frac{en_e}{B} - \frac{e^2}{\pi^2}N\frac{\Delta}{\omega_c}\left[1-\frac{(E_N-E_F)^2}{\Delta^2}\right]^{3/2} \quad . \tag{7.26}$$

7.1.4 Triangle Vertex: Additional Contributions

In Section 7.1.2, we calculated the dominant contribution $\mathbf{\Gamma}^{(q/k_F)}$ to the triangle vertex for the case of phonon drag in high, well-separated Landau levels at low temperatures. In the case of Coulomb drag, where q/k_F is small, additional contributions are of comparable or larger order of magnitude as $\mathbf{\Gamma}^{(q/k_F)}$ and it is therefore crucial not to omit them. As long as the temperature T is comparable to T_{bs} or larger, the corrections arising from additional terms generally are small for phonon drag. The situation changes, however, when $T \ll T_{bs}$, where the available momenta satisfy $q/k_F \ll 1$ so that other contributions may compete with $\mathbf{\Gamma}^{(q/k_F)}$. These additional terms stem from (i) the inclusion of vertex corrections, which lead to $1/N$-corrections and (ii) the next-to-leading order in Δ/ω_c expansion. Up to first order in $1/N$ and Δ/ω_c, the triangle vertex $\mathbf{\Gamma}$ can be written as the sum of three contributions[7]

$$\mathbf{\Gamma}(\mathbf{q},\omega) = \underbrace{\mathbf{\Gamma}^{(1/qR_c)}(\mathbf{q},\omega)}_{\text{longitudinal}} + \underbrace{\mathbf{\Gamma}^{(q/k_F)}(\mathbf{q},\omega) + \mathbf{\Gamma}^{(\Delta/\omega_c)}(\mathbf{q},\omega)}_{\text{transverse}} \quad . \tag{7.27}$$

Here, $\mathbf{\Gamma}^{(q/k_F)}$ is the conventional transverse contribution, calculated above, and $\mathbf{\Gamma}^{(1/qR_c)}$ is of first order in $1/N$ and results from including vertex corrections in the calculation of the longitudinal contribution to the triangle vertex. $\mathbf{\Gamma}^{(\Delta/\omega_c)}$ is of zeroth order in $1/N$ (as is $\mathbf{\Gamma}^{(q/k_F)}$), but contains an additional factor of Δ/ω_c with respect to $\mathbf{\Gamma}^{(q/k_F)}$. One could thus be led to the (naive) assumption that $\mathbf{\Gamma}^{(\Delta/\omega_c)}$ is negligible with respect to $\mathbf{\Gamma}^{(q/k_F)}$, since it contains an additional small factor of Δ/ω_c. However, this small factor can be compensated by a factor qR_c, which is large in the ballistic limit we are interested in.

The Contribution $\mathbf{\Gamma}^{(1/qR_c)}$

The contribution $\mathbf{\Gamma}^{(1/qR_c)}$ is purely longitudinal and stems from the inclusion of vertex corrections in the calculation of the triangle vertex. After disorder-averaging the triangle vertex within SCBA, $\mathbf{\Gamma}$ is expressed in terms of the (disorder-averaged) Green function matrix elements $G_n^{\pm}$. While disorder is already included in these matrix elements, further corrections arise for the scalar (density) vertices,[8] which lead to the replacement of $e^{i\mathbf{qr}}$ by the full vertices $\gamma^{\mu\nu}$ (see Appendix D) in the expression for $\mathbf{\Gamma}$. Here, the indices $\mu,\nu = \pm$ indicate the type of Green functions involved in the vertex. In the limit of well-separated Landau levels, the vertices are given by

$$\gamma^{\mu\nu}(\mathbf{q},\omega) \simeq \frac{1}{1 - \frac{\Delta^2}{4} e^{-q^2\ell_B^2/2} [L_N^0((q\ell_B)^2/2)]^2 G_N^{\mu}(E_F+\omega) G_N^{\nu}(E_F)} \quad . \tag{7.28}$$

To leading order in $1/qR_c$, Eq. (7.28) yields

$$\gamma^{\mu\nu}(\mathbf{q},\omega) \simeq 1 + \frac{\Delta^2}{4} e^{-q^2\ell_B^2/2} [L_N^0((q\ell_B)^2/2)]^2 G_N^{\mu}(E_F+\omega) G_N^{\nu}(E_F) \quad . \tag{7.29}$$

[7] The superscripts used to label these contributions have been chosen such that a comparison to similar contributions for the case of Coulomb drag (see Ref. [86]) is straight-forward.

[8] For white-noise disorder, it can be shown that there are no vertex corrections of the vector vertex.

Note that $\exp(-q^2\ell_B^2/2)[L_N^0((q\ell_B)^2/2)]^2$ asymptotically behaves as $1/N$. To first order in $1/N$ and Δ/ω_c, the longitudinal contributions to the triangle vertex are given by

$$\mathbf{\Gamma}_l^{(a)}(\mathbf{q},\omega) = -2\sum_{\sigma\in\{0,1\}} \hat{\mathbf{q}}\frac{\omega R_c}{2\pi^2\ell_B^2}\,\mathcal{L}_\sigma^1(q\ell_B)\mathrm{Im}[[G_N^+]^2\,\gamma_{NN}^{++}\gamma_{NN-\sigma}^{++}] \tag{7.30}$$

$$\begin{aligned}\mathbf{\Gamma}_l^{(b)}(\mathbf{q},\omega) =& 2\sum_{\sigma\in\{0,1\}} \hat{\mathbf{q}}\frac{\omega R_c}{2\pi^2\ell_B^2}\,\mathcal{L}_\sigma^1(q\ell_B)\mathrm{Im}[[G_N^+]^2\gamma_{NN}^{++}\gamma_{NN-\sigma}^{+-}\\ &- G_N^+G_N^-\gamma_{NN}^{+-}\gamma_{NN-\sigma}^{++}] \quad .\end{aligned} \tag{7.31}$$

The additional factor of two accounts for the spin degree of freedom. Here, $\gamma_{NM}^{\mu\nu} \equiv \gamma_{NM}^{\mu\nu}(\mathbf{q},\omega=0)$ are the matrix elements of the scalar vertex. To lowest order in $1/N$ and Δ/ω_c, there are no vertex corrections, i.e. all factors $\gamma^{\mu\nu}=1$. Noting that in this case the second term in the imaginary part of Eq. (7.31) is purely real due to Eq. (D-18), we then see that $\mathbf{\Gamma}_l^{(a)}$ and $\mathbf{\Gamma}_l^{(b)}$ exactly cancel each other, as mentioned above. To compute the next-order correction in $1/N$, we therefore have to include vertex corrections.

Carrying out the $(1/N)$-expansion for the vertex factors, stated in Eq. (7.29), and combining the resulting contributions of $\mathbf{\Gamma}_l^{(a)}$ and $\mathbf{\Gamma}_l^{(b)}$, we obtain

$$\begin{aligned}\mathbf{\Gamma}^{(1/qR_c)}(\mathbf{q},\omega) &= 2\sum_{\sigma\in\{0,1\}} \hat{\mathbf{q}}\frac{\omega R_c}{\pi^2\ell_B^2}\,\mathcal{L}_\sigma^1(q\ell_B)\,\mathcal{L}_0^0(q\ell_B)\,\mathrm{Im}[G_N^+]\\ &\quad\times\mathrm{Re}\left[G_N^+\left(\frac{\Delta^2}{4\,(\Sigma^-)^2}-1\right)\right] \quad .\end{aligned} \tag{7.32}$$

By using

$$\begin{aligned}\mathrm{Re}\left[G_N^+\left(\frac{\Delta^2}{4(\Sigma^-)^2}-1\right)\right] &= \mathrm{Re}\left[\frac{16}{\Delta^4}(G_N^-)^3-\frac{4}{\Delta^2}(G_N^-)^{-1}\right]\\ &= -\frac{8}{\Delta^4}(E_F-E_N)\left[\Delta^2-(E_F-E_N)^2\right]\end{aligned} \tag{7.33}$$

we obtain

$$\begin{aligned}\mathbf{\Gamma}^{(1/qR_c)}(\mathbf{q},\omega) &= -\frac{32}{\Delta^6}\hat{\mathbf{q}}\frac{\omega R_c}{\pi^2\ell_B^2}\,(E_F-E_N)\left[\Delta^2-(E_F-E_N)^2\right]^{3/2}\\ &\quad\times\sum_{\sigma\in\{0,1\}}\mathcal{L}_\sigma^1(q\ell_B)\,\mathcal{L}_0^0(q\ell_B) \quad .\end{aligned} \tag{7.34}$$

We stress again that $\mathbf{\Gamma}^{(1/qR_c)}(\mathbf{q},\omega)$ is a purely longitudinal contribution to the triangle vertex. It is interesting to note that $\mathbf{\Gamma}^{(1/qR_c)}$ is an odd function of (E_F-E_N), while the dominant contribution $\mathbf{\Gamma}^{(q/k_F)}$ is an even function of (E_F-E_N).

The Contribution $\mathbf{\Gamma}^{(\Delta/\omega_c)}$

The contribution $\mathbf{\Gamma}^{(\Delta/\omega_c)}$ is purely transverse and is the first order in Δ/ω_c correction to $\mathbf{\Gamma}^{(q/k_F)}$. To lowest order in $1/N$, vertex corrections can be neglected.

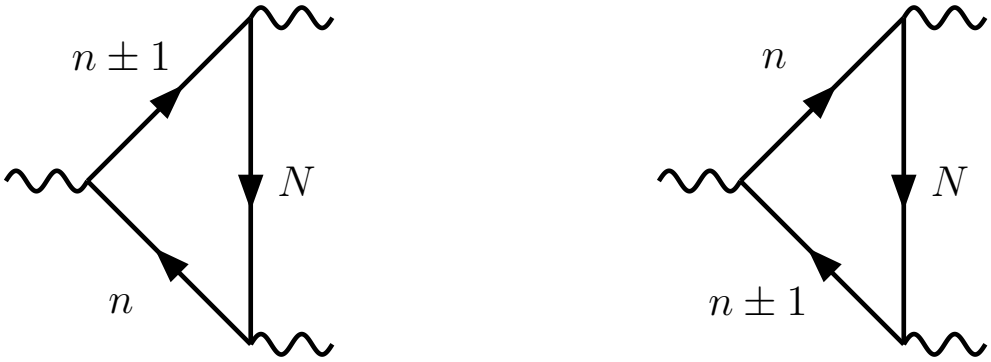

Figure 7.1: Diagrams contributing corrections of order Δ/ω_c to the triangle vertex. Here, both Green functions adjacent to the vector vertex have to be evaluated in Landau levels different from N. This figure has been taken from Ref. [86].

To lowest order in Δ/ω_c, the transverse contribution $\mathbf{\Gamma}_t^{(b)}$ yields the contribution $\mathbf{\Gamma}^{(q/k_F)}$ calculated above. To first order in Δ/ω_c, a second contribution to $\mathbf{\Gamma}_t^{(b)}$ arises, which is given by ($\mathbf{q} = q\mathbf{e}_x$)

$$\begin{aligned}\mathbf{\Gamma}^{(\Delta/\omega_c)}(\mathbf{q},\omega) &= (\mathbf{e}_z \times \hat{\mathbf{q}})\frac{8\omega R_c}{\pi^2\omega_c\Delta^4\ell_B^2}(E_F - E_N)\left[\Delta^2 - (E_F - E_N)^2\right] \\ &\quad \times \sum_{\sigma\in\{0,1\}} \mathcal{L}_\sigma^1(q\ell_B) \end{aligned} \tag{7.35}$$

It is easy to see that this contribution differs from $\mathbf{\Gamma}^{(q/k_F)}$ by a factor $(E_F - E_N)/\omega_c \sim \Delta/\omega_c$. We nevertheless may have to retain this contribution since it contains a *sum* of two vertex overlap functions, $\mathcal{L}_0^1(q\ell_B) + \mathcal{L}_1^1(q\ell_B)$, while Eq. (7.9) contains a *difference* of two vertex overlap functions, $\mathcal{L}_0^1(q\ell_B) - \mathcal{L}_1^1(q\ell_B)$, which asymptotically behaves very differently: As shown in Appendix F, the difference $\mathcal{L}_0^1(q\ell_B) - \mathcal{L}_1^1(q\ell_B)$ is small compared to the sum $\mathcal{L}_0^1(q\ell_B) + \mathcal{L}_1^1(q\ell_B)$ for $q\ell_B \ll 1$. Thus, whenever small momentum transfers play an important role, we are not allowed to omit this contribution. As for $\mathbf{\Gamma}^{(1/qR_c)}$, the contribution $\mathbf{\Gamma}^{(\Delta/\omega_c)}$ is an odd function of $(E_F - E_N)$, in contrast to the dominant contribution $\mathbf{\Gamma}^{(q/k_F)}$, which is an even function of $(E_F - E_N)$.

7.2 Interaction of 2D Electrons with Bulk Phonons in the Bilayer System

The interaction between electrons and phonons in polar semiconductors differs from the electron-phonon interaction in nonpolar materials due to the presence of piezoelectric electron-phonon interactions, as described in detail in Appendix E. In this section, we derive the phonon-mediated electron-electron interaction in a double-layer system as mimicked by a double quantum well.

7.2.1 Model

Following closely Ref. [96], we model the two layers of the bilayer system by two infinite square wells of width L and center-to-center distance $|z_1 - z_2| = d$

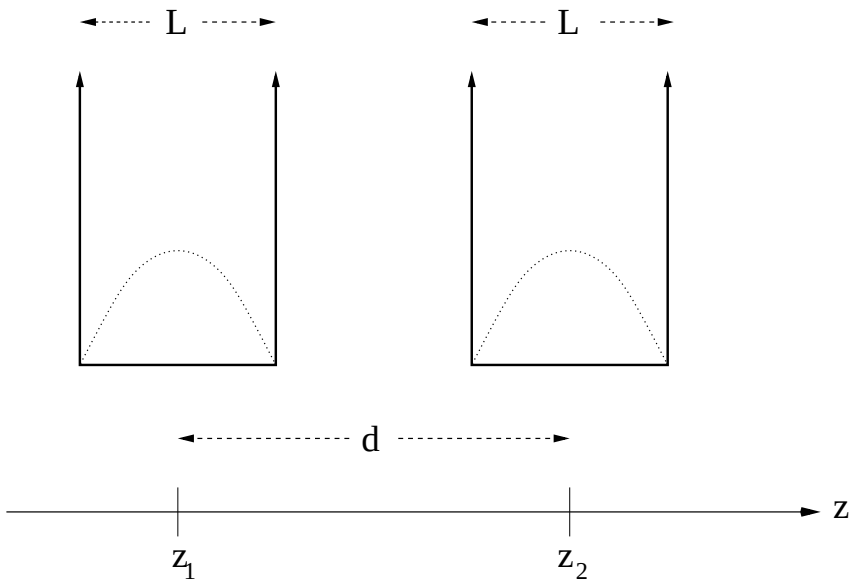

Figure 7.2: Double-layer heterostructure modeled by two narrow quantum wells with infinitely high walls. The layer planes at z_1 and z_2 are oriented in xy-direction, with thickness L and center-to-center distance d. The lowest subband wavefunctions of the two wells, $\phi_1(z)$ and $\phi_2(z)$ (indices denoting the well number, not the subband), are depicted schematically inside the wells.

(see Fig. 7.2). Due to the narrowness of the quantum wells, it is sufficient to consider only the interaction between the lowest (vertical) subbands. The lowest subband eigenfunction inside the ith square well can be approximated by [96]

$$\phi_i(z) = \sqrt{\frac{2}{L}} \sin\left[\frac{\pi}{L}\left(z - z_i + \frac{L}{2}\right)\right] \quad . \tag{7.36}$$

In the z-direction, the electrons are confined to a narrow well of width L. This can be taken into account when writing down the interaction Hamiltonian by effectively taking the expectation value in z-direction and then treating only 2D electrons interacting with phonons. To this end, it is necessary to express the 3D electron density as a function of the 2D layer density. The 3D electron density can be written as a Fourier series with coefficients

$$\rho_{\mathbf{q}} = \int d^3r e^{-i\mathbf{q}\cdot\mathbf{r}} \Psi^\dagger(\mathbf{r})\Psi(\mathbf{r}) \quad . \tag{7.37}$$

The field operators are given by

$$\Psi(\mathbf{r}) = \frac{1}{\sqrt{A}} \sum_{\mathbf{p}_\perp,\alpha} \phi_\alpha(z) e^{i\mathbf{p}_\perp\cdot\mathbf{r}} c_{\mathbf{p}_\perp,\alpha} \quad , \tag{7.38}$$

$$\Psi^\dagger(\mathbf{r}) = \frac{1}{\sqrt{A}} \sum_{\mathbf{k}_\perp,\beta} \phi^*_\beta(z) e^{-i\mathbf{k}_\perp\cdot\mathbf{r}} c^\dagger_{\mathbf{k}_\perp,\beta} \quad . \tag{7.39}$$

where A is the area of the 2D layer and $\phi_\alpha(z)$ is the (normalized) wavefunction of the α^{th} vertical subband. The vectors $\mathbf{p}_\perp$ and $\mathbf{k}_\perp$ are the projections of $\mathbf{p}$

and $\mathbf{k}$ onto the (x, y)-plane and thus are three-dimensional vectors with zero z-component. The electron density can then be written as

$$\rho_{\mathbf{q}} = \frac{1}{A}\int d^3r e^{-i\mathbf{q}\cdot\mathbf{r}} \sum_{\alpha,\beta} \phi^*_\beta(z)\phi_\alpha(z) \sum_{\mathbf{k}_\perp,\mathbf{p}_\perp} e^{i(\mathbf{p}_\perp-\mathbf{k}_\perp)\cdot\mathbf{r}_\perp} c^\dagger_{\mathbf{k}_\perp,\beta} c_{\mathbf{p}_\perp,\alpha} \quad . \tag{7.40}$$

For a narrow quantum well, only the lowest $(\alpha, \beta = 1)$ subbands are occupied. Using $\mathbf{q}\cdot\mathbf{r} = \mathbf{q}_\perp\cdot\mathbf{r}_\perp + q_z z$, one finds

$$\rho_{\mathbf{q}} = \frac{1}{A}\int dz\, |\phi_1(z)|^2\, e^{-iq_z z} \int d\mathbf{r}_\perp \sum_{\mathbf{k}_\perp,\mathbf{p}_\perp} e^{i(\mathbf{p}_\perp-\mathbf{k}_\perp-\mathbf{q}_\perp)\cdot\mathbf{r}_\perp} c^\dagger_{\mathbf{k}_\perp} c_{\mathbf{p}_\perp} \quad . \tag{7.41}$$

Next, we define the form factor $F(q_z)$ as

$$F(q_z) = \int dz\, |\phi_1(z)|^2\, e^{-iq_z z} \tag{7.42}$$

and carry out the integral over $\mathbf{r}_\perp$, which, neglecting Umklapp processes yields

$$\rho_{\mathbf{q}} = \frac{1}{A} F(q_z)\cdot A \sum_{\mathbf{k}_\perp,\mathbf{p}_\perp} \delta_{\mathbf{k}_\perp+\mathbf{q}_\perp,\mathbf{p}_\perp} c^\dagger_{\mathbf{k}_\perp} c_{\mathbf{p}_\perp} \quad . \tag{7.43}$$

After carrying out the sum over $\mathbf{k}_\perp$, we obtain

$$\rho_{\mathbf{q}} = F(q_z)\sum_{\mathbf{p}_\perp} c^\dagger_{\mathbf{p}_\perp-\mathbf{q}_\perp} c_{\mathbf{p}_\perp} = F(q_z)\rho^{2D}_{-\mathbf{q}_\perp} \quad , \tag{7.44}$$

where $\rho^{2D}_{\mathbf{q}_\perp}$ are the Fourier coefficients of the 2D layer density. The electron-phonon interaction Hamiltonian is (see Appendix E)

$$H_{ep} = \sum_{\mathbf{q}} V_{\mathbf{q}}\rho_{-\mathbf{q}} \quad . \tag{7.45}$$

Writing the interaction potential in the form of Eq. (7.46),

$$V_{\mathbf{q}} = \sum_\lambda M_\lambda(\mathbf{q})\left[a^\dagger_\lambda(-\mathbf{q}) + a_\lambda(\mathbf{q})\right] \quad , \tag{7.46}$$

where M_λ is the so-called electron-phonon matrix element, the electron-phonon interaction Hamiltonian takes the form

$$H_{ep} = \sum_{\mathbf{q}\lambda} M_\lambda(\mathbf{q}_\perp, q_z)F(q_z)\rho^{2D}_{\mathbf{q}_\perp}\left[a^\dagger_\lambda(-\mathbf{q}_\perp, -q_z) + a_\lambda(\mathbf{q}_\perp, q_z)\right] \quad , \tag{7.47}$$

where $a^\dagger_\lambda$ and a_λ are phonon creation and annihilation operators for phonons of wave vector $\mathbf{q} = (\mathbf{q}_\perp, q_z)$ and mode λ, respectively.

7.2.2 Phonon-Mediated Electron-Electron Interaction

We now adopt the following notation: We use capital letters for 3D vectors and small letters for 2D vectors, writing $\mathbf{Q} = (\mathbf{q}, Q_z)$, where $\mathbf{q}$ is the 2D vector that lies inside the (x, y)-plane. Thus, the 3D vector $\mathbf{Q}$ can be viewed as being composed by a 2D vector $\mathbf{q}$ inside the layer plane and a component Q_z perpendicular to it. Compared to the notation used in Eq. (7.47), we thus identify (left: new notation, right: notation from Section 7.2.1)

$$\mathbf{Q} = \mathbf{q} \qquad Q_z = q_z \qquad q = q_\perp \quad . \tag{7.48}$$

In this notation, the phonon Matsubara Green function is given by

$$D_\lambda\left(\mathbf{Q}, i\omega_n\right) = -\frac{2\omega_{\lambda,\mathbf{Q}}}{\left[\omega_n + \frac{c_\lambda}{2\ell_{\mathrm{ph}}}\mathrm{sgn}\left(\omega_n\right)\right]^2 + \omega_{\lambda,\mathbf{Q}}^2} \tag{7.49}$$

where ℓ_{ph} is a phenomenological phonon mean free path,[9] c_λ is the sound velocity of mode λ (longitudinal (l) or transverse (t)) and $\omega_{\lambda,\mathbf{Q}} = c_\lambda|\mathbf{Q}| = c_\lambda\sqrt{q^2 + Q_z^2}$. The phonon-mediated interaction is given by

$$\mathcal{D}_{ij}(\mathbf{q}, i\omega_n) = \int \frac{\mathrm{d}Q_z}{2\pi\hbar} \sum_\lambda |M_\lambda(\mathbf{Q})|^2 F_i(Q_z) F_j(-Q_z) D_\lambda(\mathbf{Q}, i\omega_n) \tag{7.50}$$

where i, j label the layers and $|M_\lambda(\mathbf{Q})|^2$ is the square of the electron-phonon matrix element for phonons of mode λ. The form factor $F_i(Q_z)$ of the ith well is given by

$$F_i(Q_z) = \int_{-\infty}^{\infty} \mathrm{d}z |\phi_i(z)|^2 e^{-iQ_z z} = \frac{\sin\left(\frac{LQ_z}{2}\right)}{\frac{LQ_z}{2}} \frac{1}{1 - \left(\frac{LQ_z}{2\pi}\right)^2} P_i(Q_z) \quad , \tag{7.51}$$

where $P_i(Q_z) = \exp[-iQ_z z_i]$ is a phase factor with $|P_i| = 1$.

As discussed in Appendix E, for low-energy excitations there are only acoustic phonons (in the long-wavelength limit). In a polar semiconductor such as GaAs, not only deformation potential (DP) electron-phonon scattering occurs, but also piezoelectric (PE) electron-phonon scattering. The electron-phonon interaction matrix elements for coupling to longitudinal acoustic (LA) and transverse acoustic (TA) phonons via these two scattering mechanisms appear squared in the effective electron-electron interaction and can be expressed as [91, 96, 98]

$$|M_l(\mathbf{Q})|^2 = \frac{\hbar Q}{2\rho c_l}\left[D^2 + \frac{e_{14}^2}{\mathbf{Q}^2} A_l(\mathbf{Q})\right] \quad , \tag{7.52}$$

$$|M_t(\mathbf{Q})|^2 = \frac{\hbar e_{14}^2}{2\rho c_t Q} A_t(\mathbf{Q}) \quad , \tag{7.53}$$

[9] This phonon mean-free-path is dominated by boundary scattering at low temperatures ($T \lesssim 5\mathrm{K}$) , while at higher temperatures, it is mainly due to impurity scattering and anharmonic effects like e.g. three-phonon processes [97].

where ρ is the (ionic) mass density, D the deformation potential constant and e_{14} the only nonzero entry of the piezoelectric tensor (see Appendix E). The factors $A_l(\mathbf{Q})$ and $A_t(\mathbf{Q})$ are called anisotropy factors. They usually involve an additional approximation, i.e. an averaging over the in-plane direction of $\mathbf{q}$ followed – in the case of transverse polarization – by an averaging over the two possible transverse modes. This averaging will be explained in the following section.

7.2.3 Anisotropy Factors

A suitable (orthonormalized) choice for the polarization vectors $\mathbf{e}_\lambda$ is (in spherical crystal coordinates)

$$\mathbf{e}_1 = \frac{\mathbf{Q}}{Q} = (\sin\vartheta\cos\varphi, \sin\vartheta\sin\varphi, \cos\vartheta) \quad , \tag{7.54}$$

$$\mathbf{e}_2 = (-\sin\varphi, \cos\varphi, 0) \quad , \tag{7.55}$$

$$\mathbf{e}_3 = (\cos\vartheta\cos\varphi, \cos\vartheta\sin\varphi, -\sin\vartheta) \quad . \tag{7.56}$$

The PE electron-phonon matrix elements in the zincblende structure are given by Eq. (E-56)

$$M_\lambda^{PE} = \frac{2e_{14}}{\varepsilon_0}\sqrt{\frac{\hbar}{2\rho c_\lambda Q}}\frac{q_x q_y e_{\lambda,z} + q_y Q_z e_{\lambda,x} + q_x Q_z e_{\lambda,y}}{Q^2} \quad , \tag{7.57}$$

where $e_{\lambda,i}$ is the ith cartesian component of the λth polarization vector (note that the factor of two accounts for the fact that $e_{14} = e_{123}$ in our notation, while e_{14} is frequently defined as $2e_{123}$ in the crystallographic literature). In the LA phonon case ($\lambda = 1$), the electron-phonon matrix element simplifies to

$$M_{LA}^{PE} = 2e_{14}\sqrt{\frac{\hbar}{2\rho c_l Q}}\frac{q_x q_y Q_z}{Q^3} \tag{7.58}$$

Using now $q = \left(q_x^2 + q_y^2\right)^{1/2} = Q\sin\vartheta$, M_{LA}^{PE} can be written as

$$M_{LA}^{PE} = 2e_{14}\sqrt{\frac{\hbar}{2\rho c_l Q}}\frac{3q^2 Q_z}{Q^3}\cos\varphi\sin\varphi \tag{7.59}$$

such that

$$|M_{LA}^{PE}|^2 = 4e_{14}^2\frac{\hbar}{2\rho c_l Q}\frac{9q^4 Q_z^2}{Q^6}\cos^2\varphi\sin^2\varphi \quad . \tag{7.60}$$

As an approximation, one can average over the in-plane angle φ. This yields

$$|M_{LA}^{PE}|^2 = \frac{\hbar e_{14}^2}{2\rho c_l Q}\frac{9q^4 Q_z^2}{2Q^6} \quad . \tag{7.61}$$

The combined (DP and PE) matrix element squared for interaction of electrons with LA phonons can thus be written as

$$|M_l|^2 = \frac{\hbar Q}{2\rho c_l}\left(D^2 + \frac{e_{14}^2}{Q^2}A_l\right) \tag{7.62}$$

where

$$A_l = \frac{9q^4Q_z^2}{2Q^6} \quad . \tag{7.63}$$

Next, we turn to the calculation of $|M_t|^2$, i.e. to the cases $\lambda = 2$ and $\lambda = 3$. We have

$$M_{t1} = 2e_{14}\sqrt{\frac{\hbar}{2\rho c_t Q}}\frac{q_x q_y e_{2,z} + q_y Q_z e_{2,x} + q_x Q_z e_{2,y}}{Q^2} \tag{7.64}$$

$$M_{t2} = 2e_{14}\sqrt{\frac{\hbar}{2\rho c_t Q}}\frac{q_x q_y e_{3,z} + q_y Q_z e_{3,x} + q_x Q_z e_{3,y}}{Q^2} \tag{7.65}$$

Using Eqs. (7.55) and (7.56), this yields

$$M_{t1} = 2e_{14}\sqrt{\frac{\hbar}{2\rho c_t Q}}\frac{qQ_z}{Q^2}\left(\cos^2\varphi - \sin^2\varphi\right) \tag{7.66}$$

$$M_{t2} = 2e_{14}\sqrt{\frac{\hbar}{2\rho c_t Q}}\frac{2qQ_z^3 - q^3}{Q^3}\cos\varphi\sin\varphi \tag{7.67}$$

We are interested in the matrix element of a particular phonon emitted and reabsorbed by two electrons in two different layers. Averaging over t_1- and t_2-phonon modes, we define a common matrix element for TA phonons, $M_t(\mathbf{Q})$, whose square is given by

$$\begin{aligned} |M_t|^2 &= \frac{1}{2}\left[|M_{t1}|^2 + |M_{t2}|^2\right] && (7.68)\\ &= 2e_{14}^2\frac{\hbar}{2\rho c_t Q}\left[\frac{q^2Q_z^2}{Q^4}\left(\cos^2\varphi - \sin^2\varphi\right)^2\right. \\ &\qquad \left. + \frac{\left(2qQ_z^2 - q^3\right)^2}{Q^6}\cos^2\varphi\sin^2\varphi\right] && (7.69) \end{aligned}$$

which, upon averaging, leads to

$$|M_t|^2 = e_{14}^2\frac{\hbar}{2\rho c_t Q}\frac{8q^2Q_z^4 + q^6}{4Q^6} \quad . \tag{7.70}$$

The square of the matrix element for interaction between electrons and TA phonons can then be written as

$$|M_t|^2 = e_{14}^2\frac{\hbar}{2\rho c_t Q}A_t \quad , \tag{7.71}$$

where

$$A_t = \frac{8q^2Q_z^4 + q^6}{4Q^6} \quad . \tag{7.72}$$

7.2.4 Phonon-Mediated Interlayer Interaction

The integral in Eq. (7.50) runs over all Q_z. By inspection of the integrand, it can be argued that the main contribution to the integral stems from small Q_z. As an approximation [91], it is reasonable to set $Q_z = 0$ in the anisotropy factors A_l and A_t from Eqs. (7.63) and (7.72), which are then simply

$$A_l = 0 \quad , \qquad A_t = \frac{1}{4} \quad , \tag{7.73}$$

so that the coupling constants reduce to

$$|M_l(\mathbf{Q})|^2 = \frac{\hbar Q D^2}{2\rho c_l} \quad , \qquad |M_t(\mathbf{Q})|^2 = \frac{\hbar e_{14}^2}{8\rho c_t Q} \quad . \tag{7.74}$$

In this limit, electrons scatter with LA phonons only via DP scattering and with TA phonons only via PE scattering. The interaction of LA phonons with electrons via PE scattering is completely ignored. The phonon-mediated interlayer interaction (Eq. (7.50)) can then be written as a sum of the two – longitudinal and transverse – contributions:

$$\begin{aligned} \mathcal{D}_{ij}(\mathbf{q}, i\omega_n) &= -\frac{D^2}{2\pi\rho c_l^2} \int \mathrm{d}Q_z F_i(Q_z) F_j(-Q_z) \frac{Q^2}{\left[\frac{\omega_n}{c_l} + \frac{\mathrm{sgn}(\omega_n)}{2\ell_{\mathrm{ph}}}\right]^2 + Q^2} \\ &\quad -\frac{e_{14}^2}{8\pi\rho c_t^2} \int \mathrm{d}Q_z F_i(Q_z) F_j(-Q_z) \frac{1}{\left[\frac{\omega_n}{c_t} + \frac{\mathrm{sgn}(\omega_n)}{2\ell_{\mathrm{ph}}}\right]^2 + Q^2} \end{aligned} \tag{7.75}$$

Remembering that $Q^2 = Q_z^2 + q^2$, we can write $\mathcal{D}_{ij}$ as

$$\begin{aligned} \mathcal{D}_{ij}(\mathbf{q}, i\omega_n) &= -\frac{D^2}{2\pi\rho c_l^2} \left[I^1_{ij;l}(\mathbf{q}, i\omega_n) + q^2 I^0_{ij;l}(\mathbf{q}, i\omega_n) \right] \\ &\quad -\frac{e_{14}^2}{8\pi\rho c_t^2} I^0_{ij;t}(\mathbf{q}, i\omega_n) \end{aligned} \tag{7.76}$$

where $I^\alpha_{ij;\lambda}$ is given by

$$I^\alpha_{ij;\lambda}(\mathbf{q}, i\omega_n) = \int \mathrm{d}Q_z F_i(Q_z) F_j(-Q_z) \frac{Q_z^{2\alpha}}{\left[\frac{\omega_n}{c_\lambda} + \frac{\mathrm{sgn}(\omega_n)}{2\ell_{\mathrm{ph}}}\right]^2 + Q^2} \tag{7.77}$$

It follows from Eq. (7.36) and Eq. (7.51) that the product of the form factors is

$$F_i(Q_z) F_j(-Q_z) = \frac{\sin^2\left(\frac{Q_z L}{2}\right)}{\left(\frac{Q_z L}{2}\right)^2} \frac{1}{\left[1 - \left(\frac{Q_z L}{2\pi}\right)^2\right]^2} e^{-iQ_z(z_i - z_j)} \tag{7.78}$$

Writing

$$\frac{1}{\left[\frac{\omega_n}{c_\lambda} + \frac{\mathrm{sgn}(\omega_n)}{2\ell_{\mathrm{ph}}}\right]^2 + Q^2} = \frac{1}{(Q_z + i\eta_\lambda)(Q_z - i\eta_\lambda)} \tag{7.79}$$

with

$$\eta_\lambda = \sqrt{q^2 + \left[\frac{\omega_n}{c_\lambda} + \frac{\mathrm{sgn}(\omega_n)}{2\ell_{\mathrm{ph}}}\right]^2} \tag{7.80}$$

we find

$$I^{\alpha}_{ij;\lambda}(\mathbf{q}, i\omega_n) = -\frac{1}{4}\int \mathrm{d}Q_z \frac{\left(e^{iLQ_z} + e^{-iLQ_z} - 2\right) e^{-iQ_z(z_i - z_j)}}{\left(\frac{L}{2}\right)^2 Q_z^{2-2\alpha} \left(1 - \frac{LQ_z}{2\pi}\right)^2 \left(1 + \frac{LQ_z}{2\pi}\right)^2 (Q_z + i\eta_\lambda)(Q_z - i\eta_\lambda)}$$

Evaluation of these integrals for the case $i = j$ ($(z_i - z_j) = 0$) and $i \neq j$ ($(z_i - z_j) = \pm d$) and substitution in Eq. (7.76) leads to

$$\begin{aligned} \nu_0 \mathcal{D}_{ij}(\mathbf{q}, i\omega_n) &= -\frac{3C_{DP}}{k_F L}\delta_{ij} - C_{DP}\frac{q^2 - \eta_l^2}{k_F \eta_l} B_{ij}(\eta_l d, \eta_l L/2) \\ &\quad - C_{PE}\frac{k_F}{\eta_t} B_{ij}(\eta_t d, \eta_t L/2) \end{aligned} \tag{7.81}$$

with

$$B_{ij}(x, y) = \begin{cases} \frac{\pi^2}{y^2+\pi^2}\left[\frac{3y}{2\pi^2} + \frac{1}{y} + \frac{1}{2y^2}\frac{\pi^2}{y^2+\pi^2}\left(e^{-2y} - 1\right)\right] & i = j \\ e^{-x}\left(\frac{\pi^2}{y^2+\pi^2}\right)^2 \frac{\sinh^2(y)}{y^2} & i \neq j \end{cases} \tag{7.82}$$

and

$$C_{PE} = \frac{e_{14}^2 m^*}{8\pi\hbar^2 c_t^2 \rho k_F} \quad , \tag{7.83}$$

$$C_{DP} = \frac{D^2 m^* k_F}{2\pi\hbar^2 c_l^2 \rho} \quad . \tag{7.84}$$

7.3 Analytical Results

In this section, we present analytical results for the phonon drag conductivity in the low temperature limit $T \ll \omega_c$, restricting ourselves to the main contribution originating from the contribution $\mathbf{\Gamma}^{(q/k_F)}$ to the triangle vertex. Throughout, we will assume infinitely thin electron layers ($L \to 0$). In addition, we limit the discussion to the case of an infinite phonon mean free path ℓ_{ph}. Due to the specific form of the phonon-mediated interlayer interaction, it will turn out that in this limit, piezoelectric phonon modes are most relevant. We first present an approximate analytical expression for the unscreened interlayer interaction. Since in the limit $\ell_{ph} \to \infty$ the unscreened interlayer interaction gets formally divergent, we discuss the inclusion of screening into our model. For a system with long phonon mean free paths, the screened phonon-mediated interaction is dominated by a coupled electron-phonon plasma mode. Finally, we present the analytical expression for the phonon drag conductivity in the regime of interest under study. Numerical results for a broader range of parameters will be provided in Section 7.4.

7.3.1 Unscreened Interlayer Interaction

In the limit of vanishing quantum well width ($L \to 0$) and infinite phonon mean free path ($\ell_{ph} \to \infty$), the unscreened phonon-mediated interlayer interaction $\mathcal{D}_{21}$ (see Eq. (7.81)), after analytical continuation ($i\omega_n \to \omega + i0^+$), is given by[10]

$$\nu_0 \mathcal{D}_{21}(q,\omega) \simeq -C_{\mathrm{DP}} \frac{q\,(\frac{\omega}{c_l q})^2}{k_F \sqrt{1-\frac{\omega^2}{(qc_l)^2}}} - C_{\mathrm{PE}} \frac{k_F}{q\sqrt{1-\frac{\omega^2}{(qc_t)^2}}} \tag{7.85}$$

$$\simeq -C_{\mathrm{DP}} \frac{q}{k_F \sqrt{1-\frac{\omega^2}{(qc_l)^2}}} - C_{\mathrm{PE}} \frac{k_F}{q\sqrt{1-\frac{\omega^2}{(qc_t)^2}}} \quad . \tag{7.86}$$

Here, we restricted ourselves to systems with $k_F d \gg 1$ and $d \ll d_B$ where d_B is an upper bound for the distance between the two layers, which can be determined from the condition $\mathcal{D}_{11} \simeq \mathcal{D}_{12}$, as will be explained below.

As expected, both the DP and PE parts of the interaction have poles at energies corresponding to the excitation of the respective phonons. This would lead to an infinite transconductivity, since substituting this bare interaction into our expression for the transconductivity, Eq. (6.5), would yield a $|c_\lambda q - \omega|^{-1}$ divergence in the energy transfer integral for every q. As discussed in Section 7.4, this divergence can be removed by including a finite phonon mean free path. Alternatively, the inclusion of screening has the same effect, as will be shown below.

The contributions by DP and PE interactions to the phonon-mediated interlayer interaction, Eq. (7.86), show a markedly different behavior with respect to the ratio q/k_F. While the DP-term is proportional to q/k_F, the PE-term is proportional to $(q/k_F)^{-1}$. This indicates that, depending on the momentum transfer q involved, one of them may dominate over the other, depending on the ratio q/k_F. It should also be noted that the phonon drag conductivity in principle is strongly dependent on the quantum well width L, so that no realistic conclusions about the absolute strength of the phonon drag conductivity should be drawn from our analytical study, which assumes $L \to 0$.

7.3.2 Screened Interlayer Interaction

Phonon mediated contributions to the dynamical screening function $\epsilon(q,\omega)$ are negligible for short phonon mean free paths, but become important for long phonon mean free paths [91]. In the limit $\ell_{ph} \to \infty$, we therefore cannot neglect the phonon-mediated interaction when calculating $\epsilon(q,\omega)$. The total screened interlayer interaction – comprising both the Coulomb and the phonon-mediated interactions – is given by

$$W_{21}^{tot.} = \frac{\mathcal{D}_{21}(q,\omega) + U_{21}(q,\omega)}{\epsilon(q,\omega)} \quad , \tag{7.87}$$

[10] In principle, each term in Eq. 7.86 carries an additional factor $\exp(-qd\,(1-\omega^2/(c_\lambda q)^2))$. These factors can be omitted when we restrict ourselves to interlayer separations $d \ll d_B$ as described in the main text (see Eq. (7.105)).

where, for infinitely thin electron layers, the unscreened Coulomb interlayer interaction has the form

$$\nu_0 U_{21}(q,\omega) = \nu_0 U_{21}(q) \propto \frac{e^{-qd}}{q} \quad . \tag{7.88}$$

The dynamical screening function $\epsilon(q,\omega)$ is given by

$$\begin{aligned} \epsilon(q,\omega) &= [1-(\mathcal{D}_{11}(q,\omega)+U_{11}(q))\chi_1(q,\omega)]\,[1-(\mathcal{D}_{22}(q,\omega)+U_{22}(q))\chi_2(q,\omega)] \\ &\quad -[\mathcal{D}_{21}(q,\omega)+U_{21}(q)]\,\chi_1(q,\omega)\chi_2(q,\omega) \quad , \end{aligned} \tag{7.89}$$

where $\chi_i(q,\omega)$ is the polarization function of layer i and $\mathcal{D}_{ij}(q,\omega)$ and $U_{ij}(q,\omega)$ are the *unscreened* intralayer ($i=j$) or interlayer ($i\neq j$) phonon and electron interactions, respectively. Since we are only interested in the phonon contribution to the interlayer interaction, which is strongest at momenta q near $2k_F$, and systems with $k_F d \gg 1$, we can neglect the interlayer Coulomb interaction $U_{21}(q) \propto \exp(-2k_F d)$. Assuming identical electron layers ($\chi_1=\chi_2$) of matched electron densities ($n_1=n_2$) and equal filling factor ($\nu_1=\nu_2$), we can safely assume

$$\mathcal{D}_{11}(q,\omega) = \mathcal{D}_{22}(q,\omega) \equiv \mathcal{D}(q,\omega) \tag{7.90}$$

as well as

$$U_{11}(q) = U_{22}(q) \equiv U(q) \quad . \tag{7.91}$$

In addition, we assume small layer separation $d \ll d_B$, where d_B is an upper bound for d that will be calculated self-consistently below. This enables us to equate

$$\mathcal{D}_{21}(q,\omega) \simeq \mathcal{D}(q,\omega) \quad . \tag{7.92}$$

Dropping the arguments of the interaction vertices and the polarization function for a moment, we thus find

$$\begin{aligned} \epsilon(q,\omega) &= [1-(\mathcal{D}+U)\chi][1-(\mathcal{D}+U)\chi] - \mathcal{D}^2\chi^2 \\ &= 1-2\mathcal{D}\chi-2U\chi+U^2\chi^2+2\mathcal{D}U\chi^2 \\ &= (1-U\chi)(1-U\chi-2\mathcal{D}\chi) \end{aligned} \tag{7.93}$$

We now define the dynamical electronic screening constant ϵ and the static electronic screening constant ϵ_0 via

$$\epsilon = 1+(\delta_r+i\delta_i)\,\nu_0\frac{2\pi e^2}{q} \tag{7.94}$$

and

$$\epsilon_0 = 1+\delta_r\nu_0\frac{2\pi e^2}{q} \quad , \tag{7.95}$$

with

$$\delta_r = -\frac{\mathrm{Re}[\chi(q,\omega)]}{\nu_0} \tag{7.96}$$

and

$$\delta_i = -\frac{\mathrm{Im}[\chi(q,\omega)]}{\nu_0} \quad . \tag{7.97}$$

We restrict the following discussion to the DP part of the phonon-mediated interaction, since all calculations for the PE part are strictly analogous. Using Eq. (7.93), the screened interaction vertex for the longitudinal DP coupling is approximately given by

$$\nu_0 W_{21}^l(q,\omega) \simeq \frac{-C_{\rm DP}}{\epsilon\left(\frac{k_F}{q}(\epsilon_0 + i\delta_i e^2 \frac{2\pi}{q})\sqrt{1-\frac{\omega^2}{c_l^2 q^2}} - 2C_{\rm DP}(\delta_r + i\delta_i)\right)} \quad . \tag{7.98}$$

Screening thus leads to a coupled electron-phonon mode which occurs where the real part of the denominator in the above expression vanishes, i.e. at

$$\omega_0^l = c_l q \sqrt{1 - \delta_r^2 C_{\rm DP}^2 \left(\frac{2\,q}{\epsilon_0\, k_F}\right)^2} \quad . \tag{7.99}$$

The frequency ω_0^l of the coupled mode is very close to $c_l q$. Using the value $C_{\rm DP} \simeq 1.8 \cdot 10^{-3}$ appropriate for an electron gas of electron density $n_e \simeq 2 \cdot 10^{11}$ cm^{-2}, the absolute value of the deviation of the above square root from unity is given by $2(\,q\,C_{\rm DP}\,\delta_r/k_F\epsilon_0)^2 \lesssim 8(C_{\rm DP}\,\delta_r/[1-\nu_0\delta_r 2\pi e^2/q])^2 \simeq 10^{-5} \ll 1$.

Expanding the denominator of the screened interaction vertex around its pole $\omega = \omega_0^l$, we find

$$\begin{aligned}
\nu_0 W_{21}^l(q,\omega) \;&\simeq\; -C_{\rm DP} \times \left[\epsilon\left(\frac{k_F}{q}(\epsilon_0 + i\delta_i e^2\frac{2\pi}{q})\sqrt{1-\frac{(\omega_0^l)^2}{c_l^2 q^2}} - 2C_{\rm DP}(\delta_r + i\delta_i)\right.\right. \\
&\qquad \left.\left. -\frac{k_F}{2q}\epsilon_0 \frac{(\omega-\omega_0^l)2\omega_0^l}{c_l^2 q^2\sqrt{1-\frac{(\omega_0^l)^2}{c_l^2 q^2}}}\right)\right]^{-1} \qquad (7.100) \\
&\simeq\; \left(\frac{2(c_l q)q^2}{\epsilon_0^2 k_F^2}\right) \frac{\delta_r C_{\rm DP}^2}{\epsilon\left[(\omega-\omega_0^l) + i\delta_i\delta_r C_{\rm DP}^2\left(\frac{4(c_l q)q^2}{\epsilon_0^2\epsilon k_F^2}\right)\right]} \quad . \qquad (7.101)
\end{aligned}$$

Defining the broadening of the phonon mode by

$$\Lambda_l = \delta_r\delta_i C_{\rm DP}^2 \frac{4(c_l q)q^2}{\epsilon_0^3 k_F^2} \quad , \tag{7.102}$$

we obtain for the absolute value squared of the interaction

$$\begin{aligned}
|\nu_0 W_{21}^l(q,\omega)|^2 \;&\simeq\; \frac{\delta_r}{\delta_i} C_{\rm DP}^2 \frac{(c_l q)q^2}{|\epsilon|^2\epsilon_0 k_F^2} \frac{\Lambda_l}{(\omega-\omega_0^l)^2 + \Lambda_l^2} \\
&\simeq\; \frac{\delta_r}{\delta_i} C_{\rm DP}^2 \frac{(c_l q)q^2}{|\epsilon|^2\epsilon_0 k_F^2}\; \pi\; \delta(\omega-\omega_0^l) \quad , \qquad (7.103)
\end{aligned}$$

where the second approximation is valid when

$$|\Lambda_l| \ll \left|\omega_0^l - c_l q\right| \quad ,$$

or, equivalently,

$$\delta_i/\epsilon_0 \ll \delta_r \quad ,$$

which, in general, is fulfilled for $e^2/k_F \simeq 1$.

We now turn to the calculation of the upper bound d_B for the interlayer separation, for which the above calculation is valid. In all of the above, we assumed $\mathcal{D}_{21} \simeq \mathcal{D}_{11}$. Since

$$\frac{\mathcal{D}_{21}^2(q,\omega_0)}{\mathcal{D}_{11}^2(q,\omega_0)} \simeq \exp\left(-2qd\sqrt{1-\left(\frac{\omega_0}{c_l q}\right)^2}\right) \quad , \tag{7.104}$$

this assumption can now be quantified and d_B can be calculated. For the approximation $\mathcal{D}_{21}^2(q,\omega_0) \simeq \mathcal{D}_{11}^2(q,\omega_0)$ to hold, we need

$$2qd\sqrt{1-\frac{\omega_0^2}{c_l^2 q^2}} \ll 1 \quad . \tag{7.105}$$

This results in

$$d_B \simeq \frac{k_F \epsilon_0}{2q^2 C_{\rm DP}\delta_r} \lesssim 10^2/k_F \quad . \tag{7.106}$$

It is now easy to generalize the above calculations to include also the PE phonon contributions for the screened phonon vertex. Combining the results for the DP and the PE modes, we find for the screened phonon vertex the general result

$$\begin{aligned} |\nu_0 W_{21}(q,\omega)|^2 \quad &\simeq \quad \pi\,\frac{\delta_r}{\delta_i}\left[C_{\rm DP}^2\frac{(c_l q)q^2}{|\epsilon|^2\epsilon_0\,k_F^2}\delta(\omega-\omega_0^l)\right. \\ &\qquad \left. + C_{\rm PE}^2\frac{(c_t q)k_F^2}{|\epsilon|^2\epsilon_0\,q^2}\delta(\omega-\omega_0^t)\right] \end{aligned} \tag{7.107}$$

with

$$\omega_0^l = c_l q\sqrt{1-\delta_r^2 C_{\rm DP}^2\left(\frac{2\,q}{\epsilon_0\,k_F}\right)^2} \tag{7.108}$$

and

$$\omega_0^t = c_t q\sqrt{1-\delta_r^2 C_{\rm PE}^2\left(\frac{2\,k_F}{\epsilon_0\,q}\right)^2} \quad . \tag{7.109}$$

7.3.3 Phonon Drag Conductivity

Due to its momentum dependence, it is obvious that the PE term in the screened phonon interaction, Eq. (7.107), dominates over the DP term in the *low temperature region* of the q-integration. It should be noted that in the *high temperature region*, the PE and DP terms in $|\nu_0 W_{21}(q,\omega)|^2$ become comparable. Thus, when calculating the phonon drag conductivity in the low temperature limit, it is sufficient to retain only the PE contribution to the phonon-mediated interaction and the dominant contribution $\mathbf{\Gamma}^{(q/k_F)}$ to the triangle vertex. In principle, when performing the q-integration involved in the calculation of the phonon drag conductivity for different regimes, the contributions $\mathbf{\Gamma}^{(1/qR_c)}$ and $\mathbf{\Gamma}^{(\Delta/\omega_c)}$ have to be calculated in the low temperature region whereas the contribution $\mathbf{\Gamma}^{(q/k_F)}$ has to be calculated in both the low temperature as well as

the high temperature region (at least for the case $(T\ell_B/c_t \gg 1)$). This will be performed numerically in Section 7.4.

Here, we limit ourselves to the low-temperature limit. Using Eq. (6.5), the phonon drag conductivity can be expressed as

$$\sigma_{ij}^D = \frac{e^2}{16\pi TS}\sum_{\mathbf{q}}\int_{-\infty}^{\infty}\frac{d\omega}{\sinh^2\left(\frac{\omega}{2T}\right)}\Gamma_i^{(1)}(\mathbf{q},\omega)\Gamma_j^{(2)}(\mathbf{q},\omega)|W(\mathbf{q},\omega)|^2 \quad (7.110)$$

Here, $\Gamma_i^{(j)}$ is the ith component of the triangle vertex of layer j. In the low-temperature limit, we replace the full triangle vertex by the dominant contribution $\mathbf{\Gamma}^{(q/k_F)}(\mathbf{q},\omega)$ from Eq. (7.12),

$$\mathbf{\Gamma}^{(q/k_F)}(\mathbf{q},\omega) = -\frac{16\omega}{\pi^2}\frac{\Delta^2-(E_N-E_F)^2}{\Delta^4}\mathcal{L}_0^0(q\ell_B)(\mathbf{e}_z\times\mathbf{q}) \quad . \quad (7.111)$$

The absolute value squared of the screened interlayer interaction is given by the PE part of Eq. (7.107),

$$|W_{21}(\mathbf{q},\omega)|^2 \simeq \frac{\pi}{\nu_0^2}\frac{\delta_r}{\delta_i}C_{\mathrm{PE}}^2\frac{(c_tq)k_F^2}{|\epsilon|^2\epsilon_0\,q^2}\delta(\omega-\omega_0^t) \quad (7.112)$$

with $\omega_0^t \simeq c_tq$ (see Eq. (7.109)). Using results from Section 7.1.3, δ_r and δ_i can be expressed as

$$\delta_r = 1+\frac{16\omega_c}{3\pi\Delta}\mathcal{L}_0^0(q\ell_B)\left[\frac{\Delta^2-(E_N-E_F)^2}{\Delta^2}\right]^{3/2} \quad , \quad (7.113)$$

$$\delta_i = \frac{16\omega\omega_c}{\pi\Delta^2}\mathcal{L}_0^0(q\ell_B)\left[\frac{\Delta^2-(E_N-E_F)^2}{\Delta^2}\right] \quad . \quad (7.114)$$

The interlayer interaction also contains the static and dynamic electronic screening constants $\epsilon_0 = 1+\delta_r\nu_0(2\pi e^2)/q$ and $\epsilon = \epsilon_0+i\delta_i\nu_0(2\pi e^2)/q$. Since $e^2m/\epsilon k_F \simeq 1$ under realistic experimental conditions (see e.g. Fig. 7.3 in the following section), the static dielectric constant can be approximated by $\epsilon_0 \simeq \delta_r\nu_0(2\pi e^2)/q$. From the above expressions, it is then easy to see that

$$\frac{\delta_r}{\delta_i} \propto \frac{\Delta}{\omega} \quad . \quad (7.115)$$

In the regime $T \ll c_tk_F, \Delta$, the relation $\omega \simeq T \ll \Delta$ holds. In the regime $c_tk_F \ll T \ll \Delta$, the relation $\omega \simeq c_tk_F \ll \Delta$ holds. In both regimes, we find $\delta_r \gg \delta_i$ and we can approximate the dynamic by the static screening constant, $\epsilon \simeq \epsilon_0$.

The ω-integration in Eq. (7.110) is trivial due to the delta-function in the phonon-mediated interaction, Eq. (7.112). Replacing the sum over $\mathbf{q}$ by an integral and integrating out the angular dependence in polar coordinates, we obtain (up to numerical factors)

$$\sigma_{12}^D \propto \frac{C_{\mathrm{PE}}^2(c_tk_F)^2}{e^4m^5T\Delta^2\omega_c}\frac{\Delta^2-(E_N-E_F)^2}{\Delta^2}\mathcal{J} \quad , \quad (7.116)$$

where $\mathcal{J}$ is a shorthand notation for the integral

$$\mathcal{J} = \int_0^\infty dq \frac{q^6}{\sinh^2\left(\frac{c_t q}{2T}\right)} \frac{\mathcal{L}_0^0(q\ell_B)}{\delta_r^2} \quad . \tag{7.117}$$

Note that δ_r is q-dependent (see Eq. (7.113)). The remaining task is the evaluation of $\mathcal{J}$.

This integration is performed by a scale separation between the fast oscillations in $\mathcal{L}_0^0(q\ell_B)/\delta_r^2$ and the slow variation of the remainder of the integral. Using the asymptotic expansions for the Laguerre polynomials provided in Appendix F, we find

$$\mathcal{L}_0^0(q\ell_B) \longrightarrow J_0^2(qR_c) \longrightarrow \frac{2}{\pi q R_c} \cos\left(qR_c - \frac{\pi}{4}\right) \quad . \tag{7.118}$$

The integral $\mathcal{J}$ can thus be written asymptotically as

$$\mathcal{J} \simeq \int_0^\infty dq \frac{q^6}{\sinh^2\left(\frac{c_t q}{2T}\right)} \frac{2}{\pi q R_c} \int_0^{2\pi} \frac{d\alpha}{2\pi} \frac{\cos^2(\alpha)}{\left[1 + a\cos^2(\alpha)\right]^2} \quad , \tag{7.119}$$

where $\alpha = qR_c - \pi/4$ and

$$a = \frac{16}{3} \frac{1}{\pi q R_c} \frac{\omega_c}{\Delta} \left[\frac{\Delta^2 - (E_N - E_F)^2}{\Delta^2}\right]^{3/2} = \frac{16}{3} \frac{1}{\pi q R_c} \tilde{\chi} \tag{7.120}$$

with the dimensionless broadening parameter

$$\tilde{\chi} = \frac{\omega_c}{\Delta} \left[\frac{\Delta^2 - (E_N - E_F)^2}{\Delta^2}\right]^{3/2} \quad . \tag{7.121}$$

Depending on the value of a, the integral in Eq. (7.119) takes the values

$$\int_0^{2\pi} \frac{d\alpha}{2\pi} \frac{\cos^2(\alpha)}{\left[1 + a\cos^2(\alpha)\right]^2} = \frac{1}{2(1 + a^{3/2})} \simeq \begin{cases} \frac{1}{2} & a \ll 1 \\ \frac{1}{2} a^{-3/2} & a \gg 1 \end{cases} \tag{7.122}$$

In the low-temperature regime $T \ll T_{bs} = 2c_t k_F$, the remaining q-integral is cut off by the $\sinh^2$-term and, at the upper integration boundary, a takes the value $a \simeq c_t\tilde{\chi}/(R_c T)$. This leads to

$$\mathcal{J} = \int_0^{2T/c_t} dq q^6 \frac{2}{\pi q R_c} \times \begin{cases} \frac{1}{2} & c_t\tilde{\chi} \ll R_c T \\ \frac{1}{2}(c_t\tilde{\chi}/(R_c T))^{-3/2} & c_t\tilde{\chi} \gg R_c T \end{cases} \tag{7.123}$$

For larger T in turn, more precisely in the regime $T_{bs} \ll T \ll T_\Delta = \Delta$, the remaining q-integral is cut off at $q = 2k_F$ instead of the temperature cutoff, leading to $a \simeq \tilde{\chi}/N$ at the upper integration boundary. In addition, the $\sinh^2$-term can then be expanded in its small argument, yielding

$$\frac{1}{\sinh^2\left(\frac{c_t q}{2T}\right)} \simeq \left(\frac{2T}{c_t q}\right)^2 \tag{7.124}$$

This leads to

$$\mathcal{J} = \int_0^{2k_F} dqq^6 \left(\frac{2T}{c_t q}\right)^2 \frac{2}{\pi q R_c} \times \begin{cases} \frac{1}{2} & \tilde{\chi} \ll N \\ \frac{1}{2}\left(\frac{\tilde{\chi}}{N}\right)^{-3/2} & \tilde{\chi} \gg N \end{cases} \tag{7.125}$$

Finally, we arrive at

$$\sigma_{12}^D \propto \frac{C_{\mathrm{PE}}^2 (c_t k_F)^2}{e^4 m^5 \Delta^2 \omega_c} \frac{\Delta^2 - (E_N - E_F)^2}{\Delta^2} \times \begin{cases} \frac{1}{R_c c_t^6} T^5 & T \ll T_{bs} \quad \text{and} \quad c_t\tilde{\chi} \ll R_c T \\ \frac{R_c^{1/2}}{c_t^{15/2}\tilde{\chi}^{3/2}} T^{13/2} & T \ll T_{bs} \quad \text{and} \quad c_t\tilde{\chi} \gg R_c T \\ \frac{k_F^4}{c_t^2 R_c} T & T_{bs} \ll T \ll T_\Delta \quad \text{and} \quad \tilde{\chi} \ll N \\ \frac{N^{3/2} k_F^4}{c_t^2 R_c \tilde{\chi}^{3/2}} T & T_{bs} \ll T \ll T_\Delta \quad \text{and} \quad \tilde{\chi} \gg N \end{cases} \tag{7.126}$$

For our regime of interest, $T \ll T_{bs}, T_\Delta$, only the first two cases are relevant. The latter two cases are valid for $T_{bs} \ll T \ll T_\Delta$, i.e. at temperatures exceeding T_{bs} but still below the temperature associated with the Landau level broadening. The different temperature dependence can be explained by the fact that at very low T, the available phase space for phonons is limited through temperature, while at higher T, all phonon momenta $q \leq 2k_F$ can contribute to the phonon drag conductivity. For very low T, σ_{12}^D shows a steep increase with T which turns linear at higher $T \gtrsim T_{bs}$. As our numerical studies will reveal in Section 7.4, for even higher $T \gtrsim \Delta \equiv T_\Delta$, σ_{12}^D decreases again, leading to a peak in the temperature dependence of σ_{12}^D near $T = T_\Delta$. If one were to plot the T-dependence of the drag conductivity scaled by T^{-2} as in Fig. 6.5, $\sigma_{12}^D(T)/T^2$ increases for $T < T_{bs}$, gets peaked in the vicinity of $T = T_{bs}$ and decreases for $T > T_{bs}$. The temperature dependence of phonon drag in high Landau levels thus is comparable to the temperature dependence at $B = 0$.

The most important result is that the temperature dependence of the dominant contribution to the phonon drag conductivity deviates significantly from the T^2-dependence of Coulomb drag. This deviation can be used in experiment to isolate the phonon contribution from the Coulomb contribution to frictional drag.

All expressions are valid for infinite phonon mean free path and vanishing layer thickness. Numerical results for finite layer thickness, finite phonon mean free path, higher temperatures and varying interlayer separation will be presented in the following section.

7.4 Numerical Results

In principle, results similar to Eq. (7.126) can be derived analytically for all other parameter regions, utilizing the machinery introduced in the previous

$C_{\mathrm{PE}}\, k_F = 1.64 \times 10^3/\mathrm{cm}$	,	$C_{\mathrm{PE}} \simeq 0.6 \times 10^{-3}$
$C_{\mathrm{DP}}/k_F = 2.7 \times 10^{-9}\mathrm{cm}$	,	$C_{\mathrm{DP}} \simeq 1.8 \times 10^{-3}$
$L \simeq 2 \times 10^{-6}\mathrm{cm}$	,	$Lk_F \simeq 2.7$
$d \simeq 5 \times 10^{-6}\mathrm{cm}$	,	$dk_F \simeq 6.8$
$c_l = 5.14 \times 10^5\mathrm{cm/s}$	,	$k_F/mc_l \simeq 64$
$c_t = 3.04 \times 10^6\mathrm{cm/s}$	,	$k_F/mc_t \simeq 108$
$e^2m/\epsilon = 2 \times 10^6/\mathrm{cm}$	,	$e^2m/\epsilon k_F \simeq 1.4$
$\ell_{\mathrm{ph}} \simeq 14 \times 10^{-4}\mathrm{cm}$	,	$k_F\ell_{\mathrm{ph}} \simeq 1.37 \times 10^2$

Figure 7.3: Typical experimental parameters for an electron density $n_e \simeq 2 \times 10^{11}$ cm^{-2}.

sections, thus extending our study to regimes other than the regime of interest stated in Section 7.1.1. Due to the technicality of this effort, we opt to restrict ourselves to numerical calculations. In this section, we detail the necessary extensions and generalizations to the treatment of higher temperatures, finite phonon mean free path, varying interlayer distance and Landau level broadening, mismatched layer fillings and finite layer thickness and present numerical results for realistic values of the experimental parameters, as given in the table in Fig. 7.3. Specifically, in agreement with experimental estimates, we use a finite well width of $L = 2 \times 10^{-6}$ cm. All numerical integrations involved in the calculation of the phonon drag resistivity have been performed using Monte Carlo integration, relying on routines from the GNU Scientific library GSL. Note that all numerical calculations include the full expressions for the triangle vertex and the interlayer interaction (taking into account both the DP and the PE interaction, as opposed to our analytical study in Section 7.3), thus extending our analysis beyond the regime of interest stated in Section 7.1.1.

All numerical results display the drag resistivity instead of the drag conductivity, since this is the quantity usually measured in experiment. The drag conductivity σ_{12}^D and the drag resistivity ρ_{12}^D are closely related via matrix inversion

$$\rho_{21}^D = \frac{-\sigma_{21}}{\sigma_{11}\sigma_{22} - \sigma_{12}\sigma_{21}} \quad . \tag{7.127}$$

Assuming that the intralayer conductivities σ_{11},σ_{22} are much larger than the drag conductivity ($\sigma_{21}, \sigma_{12} \ll \sigma_{11}, \sigma_{22}$), this expression is simplified to

$$\rho_{21}^D \simeq \frac{-\sigma_{21}}{\sigma_{11}\sigma_{22}} \quad , \tag{7.128}$$

where the Drude expression $\sigma_{ii} = e^2 n_i \tau_{tr_i}/m$ can be used for the intralayer conductivities (τ_{tr_i} is the transport time in the ith layer). The electronic densities n_i of the two layers are assumed to be equal, $n_1 = n_2 = n_e$. Note that in all numerical calculations, we fixed the chemical potential to $E_F = E_N$, i.e. we assumed that the Fermi level lies exactly at the center of the valence LL of index N.

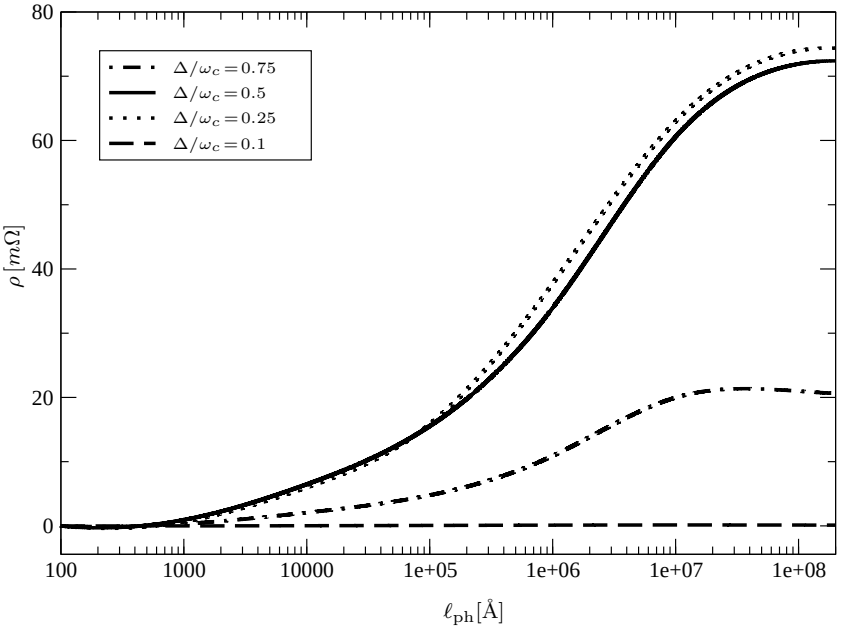

Figure 7.4: Phonon contribution to the drag resistivity ρ as a function of the phonon mean free path $\ell_{\rm ph}$ for $N = 5$, $T = 3$ K and interlayer separation $d = 500$ Å . Results are shown for four different values of the Landau level broadening parameter Δ/ω_c.

7.4.1 Finite Phonon Mean Free Path

The assumption of an infinite phonon mean free path $\ell_{\rm ph}$ is rather unrealistic: Lattice imperfections, scattering off the boundaries of the sample and anharmonic effects lead to a finite $\ell_{\rm ph}$. Since the phonon drag resistivity depends quite sensitively on the value used for $\ell_{\rm ph}$, we have to include a realistic estimate for this quantity. We therefore follow an approach similar to Ref. [91] where it has been shown that it is reasonable to split the discussion of the phonon drag resistivity to systems with either a short or a long phonon mean free path $\ell_{\rm ph}$. A system with long phonon mean free path qualitatively behaves as in the case of infinite phonon mean free path, where we have demonstrated above that the screened phonon interaction is dominated by a coupled electron-phonon plasma mode. In a system with short phonon mean free path, the phonon-mediated contributions to the polarization function $\chi(q,\omega)$ can be neglected and the electron-phonon interaction is separately screened in the two layers.

Fig. 7.4 is a logarithmic plot of the phonon contribution to the drag resistivity as a function of the phonon mean free path for four different values of the Landau level broadening parameter Δ/ω_c. For $\ell_{\rm ph} \lesssim 10^5$Å, the phonon drag resistivity ρ roughly scales logarithmically with $\ell_{\rm ph}$. This range of $\ell_{\rm ph}$ corresponds to the short phonon mean free path regime. At values $\ell_{\rm ph} \gtrsim 10^5$Å, the phonon drag resistivity increases more rapidly until it saturates at very long phonon mean free paths. The faster increase can be attributed to the emergence of the coupled electron-phonon mode. The saturation occurs when ρ approaches

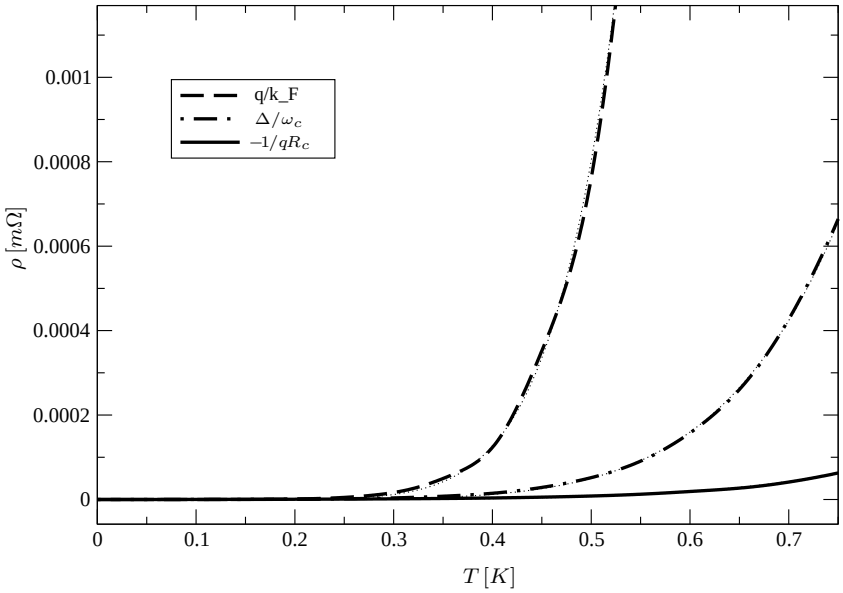

Figure 7.5: Comparison between the temperature-dependence of the different contributions ρ_{q/k_F}, ρ_{Δ/ω_c} and $-\rho_{1/qR_c}$ to the phonon drag resistivity at low temperatures T. Already at very moderate temperatures, ρ_{q/k_F} exceeds the other two contributions. In this figure, $N = 5$, $\Delta/\omega_c = 0.5$, $d = 500$ Å and $\ell_{\rm ph} = 15$ μm. Dotted curves denote a temperature-fitting of the numerical results.

its value for infinite phonon mean free path (see Eq. (7.126)), where coupling between the layers is almost exclusively mediated by the collective mode.

From here on, we choose to use the value $\ell_{\rm ph} = 15$ μm, extracted from experimental data taken at zero field [99]. Fortunately, $\ell_{\rm ph}$ hardly will be affected to any extent by the presence of the magnetic field. It is clear from the above considerations that the value $\ell_{\rm ph} = 15$ μm lies more or less at the transition between the short phonon mean free path regime and the long phonon mean free path regime. It would thus be inappropriate to employ the analytical expressions derived previously for the infinite phonon mean free path regime.

7.4.2 Temperature Dependence

In experiments without magnetic field, the phonon contribution to the total drag resistivity has been determined by comparing its temperature dependence to the expected T^2-behavior of Coulomb drag (see Chapter 6). The same can in principle be done for drag in high Landau levels, although no experiments have been conducted so far.

From the general arguments concerning the momentum dependence of the different contributions to the phonon drag conductivity in Section 7.3, we expect the contribution ρ_{q/k_F} to dominate for sufficiently high temperatures. This may be different for lower temperatures, where the other contributions – ρ_{ω/ω_c} and ρ_{1/qR_c} – can be of comparable magnitude as ρ_{q/k_F}. We recall that, in the case of Coulomb drag, where the interlayer interaction is strongly suppressed at

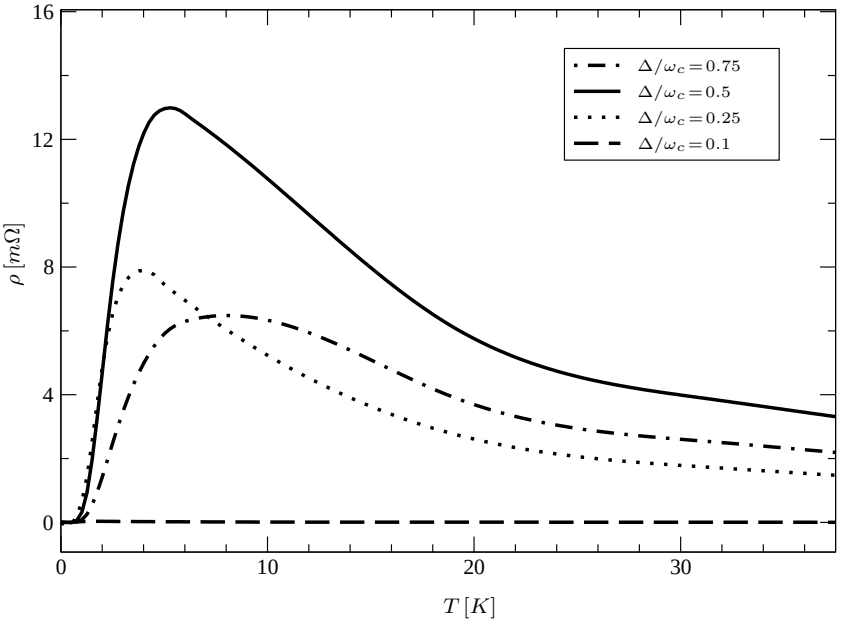

Figure 7.6: Phonon contribution to the drag resistivity ρ as a function of temperature T for different Landau level broadening parameters Δ/ω_c. The figure's temperature range extends well beyond the maximal temperatures treated in our analytical analysis of phonon drag in Section 7.3. In this figure, $N = 5$, $d = 500$ Å and $\ell_{\rm ph} = 15$ μm.

large momentum transfers, the contribution ρ_{1/qR_c} turns out to dominate over ρ_{q/k_F}. In Fig. 7.5, we display results for the three leading-order contributions ρ_{q/k_F}, ρ_{ω/ω_c} and $-\rho_{1/qR_c}$ within the low temperature regime, for the specific set of parameters $N = 5$, $\Delta/\omega_c = 0.5$ and $d = 500$ Å . As expected, we obtain that $\rho_{q/k_F} \gg \rho_{\omega/\omega_c}, \rho_{1/qR_c}$, for larger temperatures. In fact, already at quite moderate temperatures $T \gtrsim 0.5$ K, the contribution ρ_{q/k_F} greatly exceeds the other two contributions. Only for very low temperatures, where all three contributions become very small, the additional contributions are of comparable magnitude, so that all three have to be retained in the calculation of the drag resistivity. In addition, our numerical results suggest different temperature scaling of the additional contributions with respect to the temperature dependence of ρ_{q/k_F}, as expected from our general arguments in Section 7.3.

In Fig. 7.6, the phonon drag resistivity ρ is plotted as a function of temperature T. At very low temperatures ($T \lesssim 1$ K), we observe that $\rho(T)$ scales with a high power of T. At higher temperatures (1 K $\lesssim T \lesssim 5$ K), the temperature dependence is observed to get roughly linear. This is in good agreement with expectations based on our previous analytical studies (see Eq. (7.126)). Fig. 7.6, however, extends the temperature range well beyond the analytically-studied temperature range $T \ll T_{bs}$. For higher temperatures ($T \gtrsim 5$ K), $\rho(T)$ reaches a peak and then decreases slowly with T. In addition, we find a strong dependence on the value of the Landau level broadening parameter Δ/ω_c, although the qualitative behavior of $\rho(T)$ is the same for all four values of Δ/ω_c. The

dependence on the Landau level broadening parameter will be studied in the following section.

Combining our insights from the analytical study in Section 7.3 and the present numerical results, we can conclude on the following scenario for the temperature dependence of the drag resistivity: There are two characteristic temperatures, one associated with the Landau level broadening

$$T_\Delta := \Delta \simeq \frac{\Delta}{\omega_c}\frac{1}{N} \times 125 \text{ K} \quad , \tag{7.129}$$

and one associated with the maximal momentum exchange,

$$T_{bs} := 2ck_F \simeq 6 \text{ K} \quad . \tag{7.130}$$

The numerical values in the above expressions have been calculated for an electronic density of $n_e \simeq 2 \times 10^{11}\text{cm}^{-2}$. As long as $T < \min[T_\Delta, T_{bs}]$, the phonon drag resistivity increases strongly with T. Let us assume $T_{bs} < T_\Delta$, in accordance with our numerical parameters. For $T_{bs} \ll T \ll T_\Delta$, the increase becomes roughly linear. For temperatures $T \gg T_\Delta$, the phonon drag resistivity decreases as a function of T. This leads to a peak in the phonon drag resistivity at about $T = T_\Delta$. Fig. 7.6 shows qualitative agreement with this scenario.

7.4.3 Dependence on Landau Level Broadening

As already indicated by the numerical study of the temperature dependence of the phonon drag resistivity ρ, there also is a pronounced dependence on the specific value of the Landau level broadening parameter Δ/ω_c (see Fig. 7.6). In Fig. 7.7, we display results for the dependence $\rho(\Delta/\omega_c)$ at five different temperatures. It turns out that ρ depends nonmonotonically on Δ/ω_c. It first increases as a function of Δ/ω_c for small Δ/ω_c and then decreases again for large values of Δ/ω_c, reaching its maximum at $\Delta/\omega_c \simeq 1/3$. In addition, we observe a very strong suppression of ρ at low values of Δ/ω_c as opposed to a rather slow decrease at high values of Δ/ω_c.

This can be explained through inspection of the momentum cutoffs involved in the integrals for the phonon drag resistivity. Denote by Δ^* the broadening where $T_\Delta = T_{bs}$. This broadening is approximately given by

$$\frac{\Delta^*}{\omega_c} = 4\frac{Ncm}{k_F} \simeq \frac{N}{20} \quad . \tag{7.131}$$

We find that for $\Delta \ll \Delta^*$ the momentum cutoff of the integrals involved in the calculation of the drag conductivity is determined by Δ/c. The drag resistivity then scales with a very high power of Δ for $T \gg \Delta$, explaining the strong suppression observed for $\Delta \ll \Delta^*$ in Fig. 7.7. For $\Delta \gg \Delta^*$, as suggested by Eq. (7.126), we obtain a slower decrease of the phonon drag resistivity with Δ/ω_c.[11]

[11] Note that, in Eq. (7.126), the dimensionless broadening parameter $\tilde{\chi}$ is proportional to Δ/ω_c.

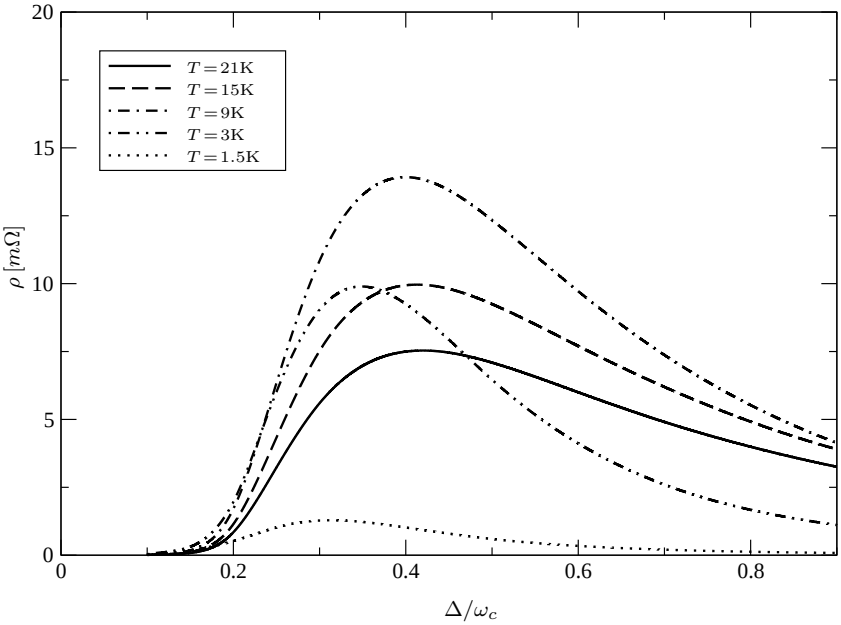

Figure 7.7: Phonon contribution to the drag resistivity ρ as a function of the Landau level broadening Δ/ω_c for different temperatures T. In this figure, the system parameters are $N = 5$, $\ell_{\rm ph} = 15$ μm and $d = 500$ Å.

7.4.4 Dependence on Interlayer Separation

In principle, it is possible to manufacture a series of nearly-identical double-quantum-well systems with different interlayer separations [90, 100, 99]. Drag measurements on such a series would yield further valuable insight into the specific nature of the phonon-mediated interaction.

Fig. 7.8 constitutes a logarithmic plot of the drag resistivity as a function of the interlayer separation d for different Landau level broadening parameters Δ/ω_c. Our numerical study reveals an interesting nearly-logarithmic dependence

$$\rho \sim -\log(d) \tag{7.132}$$

of the phonon drag resistivity ρ on the interlayer separation. This logarithmic dependence persists over a fairly wide range of interlayer separations 100 Å $\ll d \ll$ 5000 Å. This is in qualitative agreement with experimental results [99] and theoretical predictions [91] at *zero* magnetic field.[12] Again, we observe a non-monotonic dependence of the drag resistivity on the Landau level broadening over the whole range of interlayer separations.

[12] In the experiment of Ref. [99], the values for the phonon mean free path were determined by fitting the measured drag conductivity to the theoretical predictions for the short mean free path regime from Ref. [91].

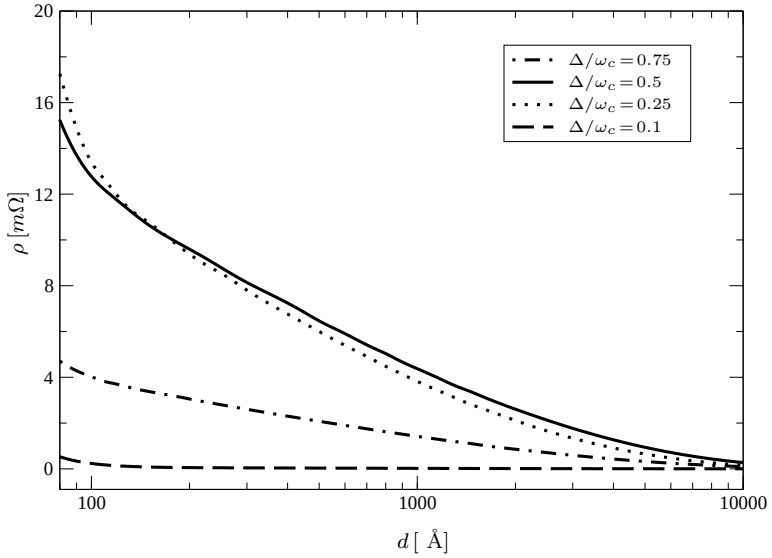

Figure 7.8: Logarithmic plot of the drag resistivity ρ as a function of the interlayer separation d for a number of values of the Landau level broadening parameter Δ/ω_c. All results have been obtained at temperature $T = 3$ K and for Landau level index $N = 5$. The phonon mean free path has been chosen $\ell_{\rm ph} = 15$ μm.

7.4.5 Filling Factor Dependence: Equal Filling Factors

Experiment allows for a separate variation of the filling factors of the 2DEG electron layers in a bilayer system. In the case of Coulomb drag, interesting effects have been observed for different filling factors in the regime of weak interlayer coupling, the most notable of which is the emergence of negative drag [82, 83], contradicting earlier theoretical predictions of strictly positive drag [101, 92]. In this section, we present numerical results for the dependence of the phonon drag resistivity on the filling factor at equal filling $N_1 = N_2 = N$ of the two layers of the bilayer system. The subsequent section studies the behavior at different filling.

Fig. 7.9 shows the rescaled drag resistivity $N^2\rho$ as a function of the common filling factor N for different values of the Landau level broadening at temperature $T = 3$ K for matched densities $n_1 = n_2$. In close analogy to previous considerations, we define the Landau level filling N^* by the condition $T_\Delta = T_{bs}$. It is given by

$$N^* = \frac{k_F}{4mc}\frac{\Delta}{\omega_c} \simeq 20\frac{\Delta}{\omega_c} \quad . \tag{7.133}$$

Due to the scaling of the phonon contribution to the drag resistivity (see Eq. (7.126)), we expect a turning point in $N^2\rho$ in the vicinity of N^*, where the behavior changes from an increasing curve for $N \ll N^*$ to a decreasing curve for $N \gg N^*$. This is in agreement with Fig. 7.9. Note that the actual value of the Landau level index at which this transition happens is approximately $N^*/3$ larger than the value of N^* predicted by Eq. (7.133). This can be readily ex-

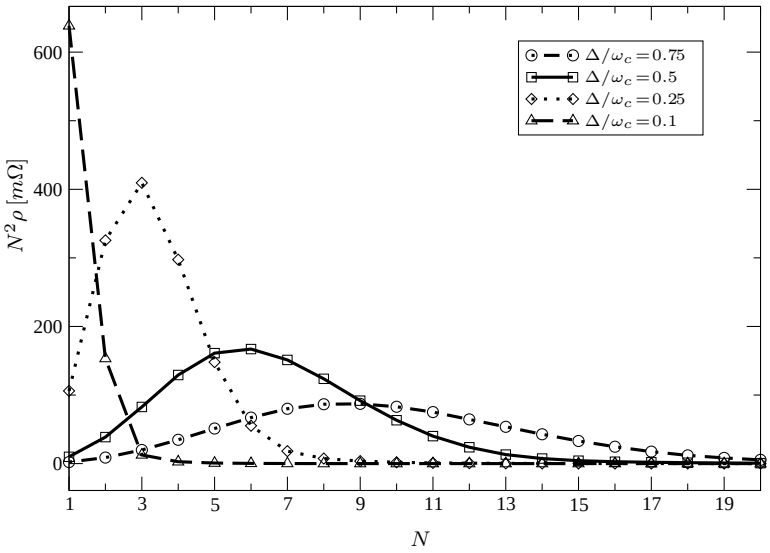

Figure 7.9: Rescaled drag resistivity $N^2\rho$ as a function of the Landau level index for different broadening parameters Δ/ω_c. The results shown have been calculated for the parameters $T = 3$ K, $d = 500$ Å and $\ell_{\rm ph} = 15$ μm

plained by the uncertainty in the determination of the effective phonon velocity c from c_l and c_t.

7.4.6 Filling Factor Dependence: Different Filling Factors

Up to this point, we assumed identical 2DEG layers with equal filling. As mentioned above, experiment allows for different filling factors in the two layers. We expect a strong dependence of the phonon drag resistivity on the ratio of the filling factors in both layers. We calculated the phonon contribution to the rescaled drag resistivity $N_1 N_2 \rho$ numerically for general fillings N_1 and N_2, which are close to each other ($N_1 \simeq N_2$). Fig. 7.10 shows numerical results for the phonon drag resistivity at fixed $N_1 = 5$ as a function of N_2 for four different values of the Landau level broadening. As expected, the drag resistivity decreases away from equal fillings. Unlike in the case of Coulomb drag, however, no sign change is observed in the phonon drag resistivity away from equal fillings.

7.5 Discussion

In this chapter, we developed the linear response theory for phonon drag in high Landau levels, extending the well-established approach for Coulomb drag of Ref. [86]. The phonon-mediated interlayer interaction differs from the Coulomb interaction by allowing for arbitrary momentum transfers $0 < q < 2k_F$ instead of only small momentum transfers. We were able to demonstrate analytically that this momentum dependence entails a temperature dependence of the

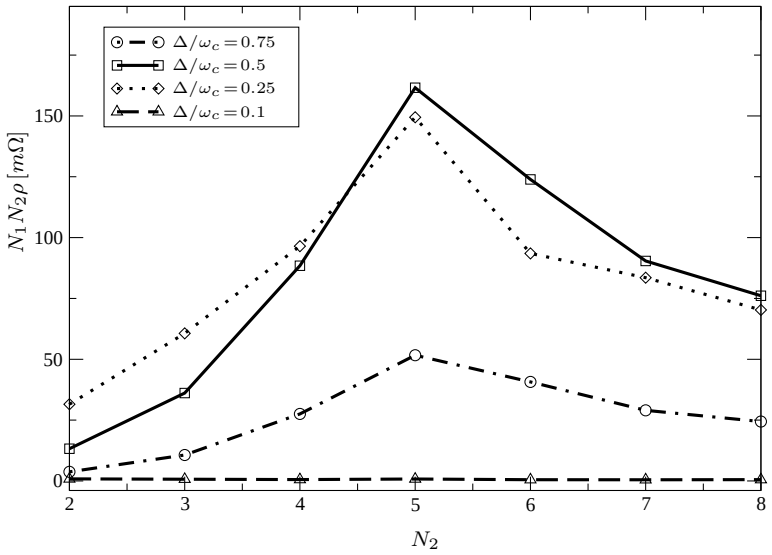

Figure 7.10: Rescaled drag resistivity $N_1 N_2 \rho$ for matched densities and different filling factors N_1 and N_2. Here, we fixed $N_1 = 5$ and calculated the rescaled drag resistivity as a function of N_2 for different broadening parameters Δ/ω_c. The system parameters are given by $T = 3$ K, $d = 500$ Å and $\ell_{\rm ph} = 15$ μm.

phonon-mediated contribution to the drag conductivity which differs strongly from the T^2-dependence of the Coulomb contribution. The behavior of the phonon drag conductivity is governed by two characteristic temperatures. As long as temperatures are small compared to T_{bs}, i.e. to the temperature at which momenta of the order of $2k_F$ can be transferred from one layer to the other via the phonon-mediated interaction, the phonon drag conductivity grows with a large power of T. The T-dependence gets linear for temperatures in between T_{bs} and T_Δ, where the latter is a measure of the disorder broadening of the Landau band. From our numerical studies, we find a decrease for temperatures exceeding T_Δ. This temperature dependence can be explained by the fact that at very low T, the available phase space for phonons is limited through temperature, while at higher T, all phonon momenta $q \leq 2k_F$ can contribute to the phonon drag conductivity. As was done for zero magnetic field, the differences in the temperature dependence of phonon vs. Coulomb drag can be used to separate these effects in experimental studies, which remain to be carried out.

Furthermore, our numerical studies revealed interesting behavior of the phonon drag resistivity with respect to the phonon mean free path, the Landau level broadening, the interlayer separation and the filling factor of the layers of the bilayer system. Very interestingly, for different filling of the layers, no sign change of the phonon drag conductivity is found, in contrast to the case of Coulomb drag. This can be attributed to the fact that the dominant contribution to the triangle vertex, $\mathbf{\Gamma}^{(q/k_F)}$, is even with respect to the chemical potential $(E_F - E_N)$ (see Eq. (7.12)), while, for Coulomb drag, the dominant contributions are odd (see Eqs. (7.34-7.35)).